Synchronous volcanic eruptions and abrupt climate change ~17.7 ka plausibly linked by stratospheric ozone depletion

Joseph R. McConnell[a,1], Andrea Burke[b], Nelia W. Dunbar[c], Peter Köhler[d], Jennie L. Thomas[e], Monica M. Arienzo[a], Nathan J. Chellman[a], Olivia J. Maselli[a], Michael Sigl[a], Jess F. Adkins[f], Daniel Baggenstos[g], John F. Burkhart[h], Edward J. Brook[i], Christo Buizert[i], Jihong Cole-Dai[j], T. J. Fudge[k], Gregor Knorr[d], Hans-F. Graf[l], Mackenzie M. Grieman[m], Nels Iverson[c], Kenneth C. McGwire[n], Robert Mulvaney[o], Guillaume Paris[f], Rachael H. Rhodes[i,p], Eric S. Saltzman[m], Jeffrey P. Severinghaus[g], Jørgen Peder Steffensen[q], Kendrick C. Taylor[a], and Gisela Winckler[r]

[a]Division of Hydrologic Sciences, Desert Research Institute, Reno, NV 89512; [b]School of Earth and Environmental Sciences, University of St. Andrews, St. Andrews, KY16 9AL United Kingdom; [c]New Mexico Institute of Mining and Technology, Socorro, NM 87801; [d]Alfred-Wegener-Institut Helmholtz-Zentrum für Polar- und Meeresforschung, 27512 Bremerhaven, Germany; [e]Sorbonne Université, Pierre and Marie Curie University, Université Versailles St-Quentin, CNRS, Institut National des Sciences de l'Univers, Laboratoire Atmosphères, Milieux, Observations Spatiales, Institut Pierre Simon Laplace, 75252 Paris, France; [f]Division of Geological and Planetary Sciences, California Institute of Technology, Pasadena, CA 91125; [g]Scripps Institution of Oceanography, University of California, San Diego, La Jolla, CA 92093; [h]Department of Geosciences, University of Oslo, NO-0316 Oslo, Norway; [i]College of Earth, Ocean, and Atmospheric Sciences, Oregon State University, Corvallis, OR 97331; [j]Department of Chemistry and Biochemistry, South Dakota State University, Brookings, SD 57007; [k]Department of Earth and Space Sciences, University of Washington, Seattle, WA 98195; [l]Centre for Atmospheric Science, University of Cambridge, Cambridge, CB2 3EN United Kingdom; [m]Department of Earth System Science, University of California, Irvine, CA 92617; [n]Division of Earth and Ecosystem Sciences, Desert Research Institute, Reno, NV 89512; [o]British Antarctic Survey, Cambridge, CB3 OET United Kingdom; [p]Department of Earth Sciences, University of Cambridge, Cambridge, CB2 3EQ United Kingdom; [q]Centre for Ice and Climate, University of Copenhagen, Copenhagen, DK-1017 Denmark; and [r]Lamont-Doherty Earth Observatory, Earth Institute at Columbia University, Palisades, NY 10964

Edited by Wallace S. Broecker, Columbia University, Palisades, NY, and approved August 7, 2017 (received for review April 5, 2017)

Glacial-state greenhouse gas concentrations and Southern Hemisphere climate conditions persisted until ~17.7 ka, when a nearly synchronous acceleration in deglaciation was recorded in paleoclimate proxies in large parts of the Southern Hemisphere, with many changes ascribed to a sudden poleward shift in the Southern Hemisphere westerlies and subsequent climate impacts. We used high-resolution chemical measurements in the West Antarctic Ice Sheet Divide, Byrd, and other ice cores to document a unique, ~192-y series of halogen-rich volcanic eruptions exactly at the start of accelerated deglaciation, with tephra identifying the nearby Mount Takahe volcano as the source. Extensive fallout from these massive eruptions has been found >2,800 km from Mount Takahe. Sulfur isotope anomalies and marked decreases in ice core bromine consistent with increased surface UV radiation indicate that the eruptions led to stratospheric ozone depletion. Rather than a highly improbable coincidence, circulation and climate changes extending from the Antarctic Peninsula to the subtropics—similar to those associated with modern stratospheric ozone depletion over Antarctica—plausibly link the Mount Takahe eruptions to the onset of accelerated Southern Hemisphere deglaciation ~17.7 ka.

climate | deglaciation | volcanism | ozone | aerosol

Long-term variations in global climate, such as the glacial/interglacial cycles recorded in paleoarchives, are linked to changes in Earth's orbital parameters and insolation (1). Superimposed on this smooth, orbital-scale variability are abrupt changes in climate, resulting in substantial variations among glacial terminations (2) and suggesting that the evolution of each deglaciation may be influenced by climate drivers specific to that deglaciation (3). One such rapid change during the last termination began ~17.7 ky before 1950 (17.7 ka), when paleoclimate records show sharp, nearly synchronous changes across the Southern Hemisphere (SH) such as a widespread retreat of glaciers in Patagonia (4, 5) and New Zealand (6), onset of rapid lake expansion in the Bolivian Andes (7), increases in summertime precipitation in subtropical Brazil (8), decreases in southern Australian aridity (9), and dust deposition recorded in ocean sediment cores (9, 10) (Fig. 1). At the same time, Antarctic ice cores record a sharp decrease in SH continental dust (11), a widespread decline in sea salt deposition, a marked upturn in water isotopic ratios indicating warming (12, 13), and a trend of increasing atmospheric methane (CH_4) (12) and carbon dioxide (CO_2) (14, 15) coincident with a drop in the stable carbon isotopic ratios in CO_2 (14) (Fig. 1). Although the causes are not certain, many of these rapid changes have been attributed to a sudden poleward shift in the westerly winds encircling Antarctica, with resulting changes in SH hydroclimate, sea ice extent, ocean circulation (6, 7, 9), and ventilation of the deep Southern Ocean (16).

The new very high time resolution West Antarctic Ice Sheet (WAIS) Divide (WD) (12) ice core record from West Antarctica (*Materials and Methods*) shows that, following a long period of relative stability extending glacial-state climate conditions [>10 ky after

Significance

Cold and dry glacial-state climate conditions persisted in the Southern Hemisphere until approximately 17.7 ka, when paleoclimate records show a largely unexplained sharp, nearly synchronous acceleration in deglaciation. Detailed measurements in Antarctic ice cores document exactly at that time a unique, ~192-y series of massive halogen-rich volcanic eruptions geochemically attributed to Mount Takahe in West Antarctica. Rather than a coincidence, we postulate that halogen-catalyzed stratospheric ozone depletion over Antarctica triggered large-scale atmospheric circulation and hydroclimate changes similar to the modern Antarctic ozone hole, explaining the synchronicity and abruptness of accelerated Southern Hemisphere deglaciation.

Author contributions: J.R.M. designed research; J.R.M., A.B., N.W.D., P.K., J.L.T., M.M.A., N.J.C., O.J.M., M.S., J.F.A., D.B., J.F.B., E.J.B., J.C.-D., T.J.F., G.K., M.M.G., N.I., K.C.M., R.M., G.P., R.H.R., E.S.S., J.P. Severinghaus, J.P. Steffensen, K.C.T., and G.W. performed research; J.R.M. contributed new reagents/analytic tools; J.R.M., A.B., N.W.D., P.K., J.L.T., M.S., E.J.B., C.B., J.C.-D., G.K., H.-F.G., N.I., K.C.M., and G.W. analyzed data; and J.R.M., A.B., N.W.D., P.K., J.L.T., E.J.B., C.B., H.-F.G., and G.W. wrote the paper.

The authors declare no conflict of interest.

This article is a PNAS Direct Submission.

Freely available online through the PNAS open access option.

Data deposition: The data reported in this work have been deposited with the U.S. Antarctic Program Data Center, www.usap-dc.org/view/dataset/601008.

[1]To whom correspondence should be addressed. Email: Joe.McConnell@dri.edu.

This article contains supporting information online at www.pnas.org/lookup/suppl/doi:10.1073/pnas.1705595114/-/DCSupplemental.

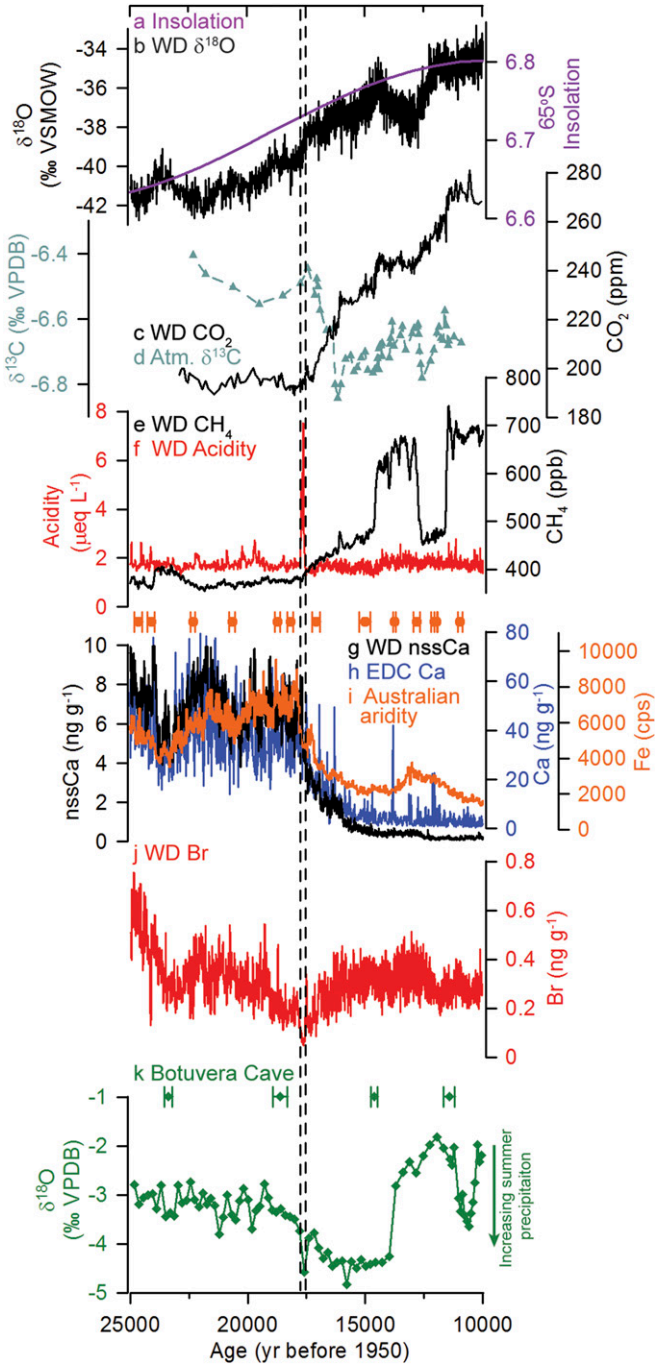

Fig. 1. Changes in climate indicators during the last glacial termination relative to the 17.7 ka glaciochemical anomaly. Shading shows the ∼192-y glaciochemical anomaly. (*A*) Annually integrated (12) 65°S insolation and (*B*) WD $\delta^{18}O$ (12); (*C*) WD CO_2 (15) and (*D*) Taylor Glacier $\delta^{13}C$ of CO_2 synchronized to the WD CO_2 record (46); (*E*) WD CH_4 (60) and (*F*) WD mineral acidity; SH dust proxies (*G*) nssCa in the WD core, (*H*) Ca in the European Project for Ice Coring in Antarctica Dome C (EDC) (11) synchronized to WD using volcanic events, and (*I*) Fe in a South Australian ocean sediment core (9); (*J*) the surface UV indicator Br in the WD core; and (*K*) Botuvera speleothem $\delta^{18}O$ that is a proxy for summertime precipitation in southeastern Brazil (8).

the 65°S annually integrated insolation minimum marking the Last Glacial Maximum (LGM)], sea salt and SH continental dust aerosol concentrations, snowfall rates, water isotope ratios, and greenhouse gas concentrations [CO_2 (15), CH_4] changed at 17.7 ka or soon after, sharply at first and then more gradually (Fig. 1). Concentrations of the traditional continental dust tracer non-sea-salt calcium (nssCa) dropped 100-fold, from ∼7 ng·g^{-1} during the LGM to ∼0.07 ng·g^{-1} during the early Holocene, with nearly 50% of the total decrease occurring during the 400 y after 17.7 ka. Sea-salt sodium concentration (ssNa), thought to be a proxy for sea ice formation, decreased fivefold during the deglaciation, with ∼40% of the decline occurring in this same period (12). About 25% of the ∼8‰ $\delta^{18}O$ and 10% of the 320 parts-per-billion CH_4 overall increases from LGM to the early Holocene values happened during these 400 y (12) (Fig. 1).

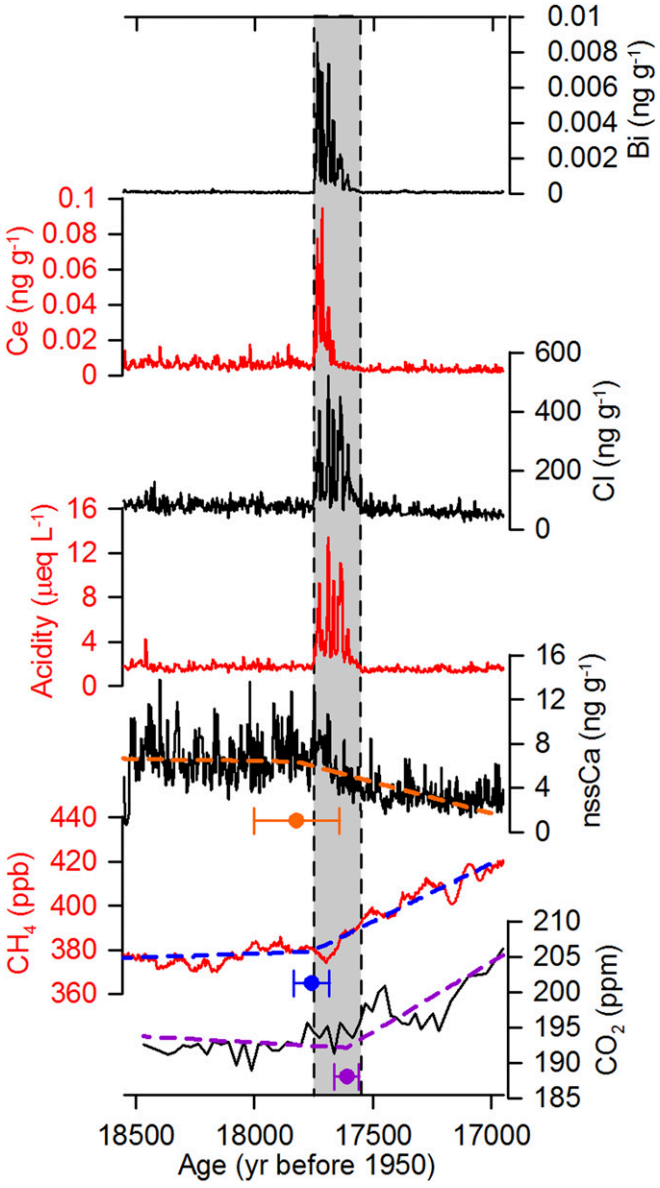

Fig. 2. Selected high-resolution elemental and gas phase measurements through the ∼192-y glaciochemical anomaly in the WD ice core at 17.7 ka (gray shading) showing nine distinct pulses. Acidity, low-boiling-point heavy metals (e.g., Bi), and halogens (e.g., Cl) other than Br (Fig. 1) were highly elevated throughout the anomaly (*SI Appendix*, Fig. S1), with REE (e.g., Ce) enhanced only during the first ∼120 y. SH dust indicators (e.g., nssCa) were elevated only slightly, and slowly increasing greenhouse gas [CH_4 (60), CO_2 (15)] concentrations accelerated during the event (Fig. 1). Measurements in the Byrd core are similar (*SI Appendix*, Fig. S2). Calculated break points (1σ uncertainty) suggest that long-term changes in nssCa, CH_4, and CO_2 concentrations in the WD core began during the 17.7 ka anomaly (*Materials and Methods*).

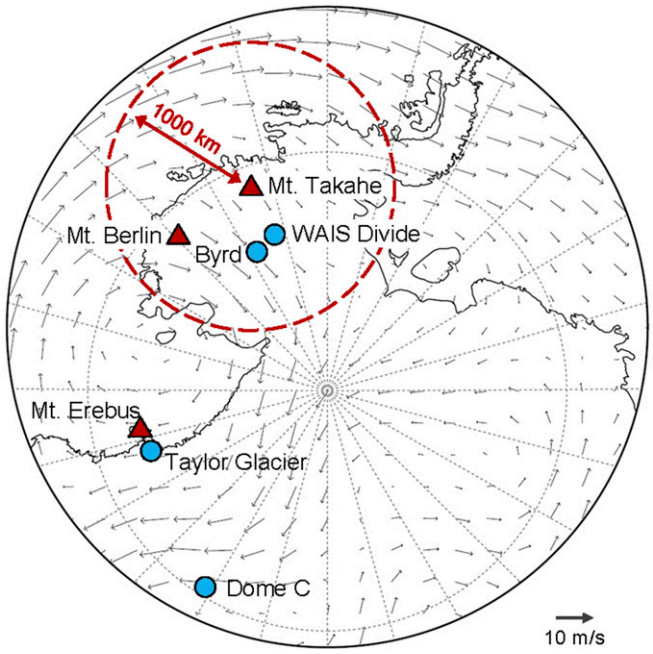

Fig. 3. Spatial extent of the glaciochemical anomaly. Evidence of the ~192-y anomaly has been found >2,800 km from Mount Takahe in ice core (circles) chemical records (*SI Appendix*, Fig. S3) as well as radar surveys from much of West Antarctica. Also shown are area volcanoes (triangles). September/October horizontal wind vectors at 600 hPa based on 1981–2010 National Centers for Environmental Prediction reanalysis fields show transport patterns consistent with observations.

Measurements of nssCa and other SH dust proxies in the WD core (Figs. 1 and 2) (*SI Appendix*, Fig. S1)—complemented by new measurements (Dataset S1) in archived samples of the Byrd core (17) located 159 km from WD (Fig. 3) (*SI Appendix*, Fig. S2)—indicate that the abrupt climate change started in central West Antarctica ~17.7 ka, with the sharp and sustained decline in SH continental dust deposition (Fig. 1) nearly synchronous (*SI Appendix*, *Continuous Ice Core Measurements*) with the start of marked increases in CH_4 and CO_2 (Fig. 2). Starting ~60 (±18) y before the abrupt drop in dust and extending ~132 y after was a unique, long-lived glaciochemical anomaly originally detected in limited discrete measurements of acidity, chloride, and fluoride in the Byrd core (17) (*SI Appendix*, Fig. S3). New continuous measurements of a broad range of elements and chemical species in the WD and Byrd cores (*SI Appendix*, Figs. S1 and S2) show that the glaciochemical anomaly consisted of nine pulses measured between 2,426.97 m and 2,420.04 m depth in the WD core, corresponding to a ~192-y period from 17.748 ka to 17.556 ka (Fig. 2) on the WD2014 timescale (18). Evidence of this glaciochemical anomaly also has been traced throughout West Antarctica and parts of East Antarctica in ice cores (17) (Fig. 3) (*SI Appendix*, Fig. S3) and radar surveys (19).

Mount Takahe 17.7 ka Volcanic Event

Elements and chemical species associated with seawater (e.g., sodium, magnesium, calcium, strontium), fallout from biomass burning (e.g., black carbon, ammonium, nitrate), and continental dust (e.g., aluminum, calcium, vanadium, iron, rubidium, barium) showed little or no change during the glaciochemical anomaly in both the WD and Byrd cores (*SI Appendix*, Figs. S1 and S2). Other elements increased by up to 50 times background concentrations, however, including rare earth elements (REE) that normally are associated with insoluble particles and low-boiling-point heavy metals linked, in past studies, to Antarctic volcanic emissions (20). Concentration changes differed between elements (*SI Appendix*, Figs. S1 and S2), with increases above background levels during nine distinct pulses of 1.7-fold for sulfur; up to sixfold for chlorine; 10-fold for lead; 20-fold for cerium, lanthanum, and thallium; and 50-fold for bismuth. While no increases were observed in the smaller (0.8 μm to 2.4 μm) insoluble particle size fraction, 2.5- and 11-fold increases were found for the medium (2.4 μm to 4.5 μm) and larger (4.5 μm to 9.5 μm) fractions, respectively (*SI Appendix*, Fig. S1). Of all of our ~35 chemical measurements, only bromine and bromide concentrations (*SI Appendix*, *Bromine and Bromide*) declined during this ~192-y period (Fig. 1) (*SI Appendix*, Figs. S1 and S2).

Consistent with the initial interpretation of the original Byrd measurements (17) but in contrast to subsequent interpretations (21) (*Materials and Methods*), the very pronounced enrichments of low-boiling-point heavy metals (20) and halogens (22), as well as elevated concentrations of medium and larger insoluble particle fractions in the WD core (Fig. 2) (*SI Appendix*, Fig. S1), clearly indicate a volcanic source for the glaciochemical anomaly (23). Although sulfur during the anomaly was relatively low (Fig. 4), the S/Cl mass ratio was ~0.1, which is nearly identical to the 0.095 ratio reported for modern emissions from nearby Mount Erebus (23). Moreover, tephra particles from the anomaly (*Materials and Methods*), analyzed by electron microprobe, showed mineralogy of a trachytic volcanic eruption (*SI Appendix*, Table S1) geochemically consistent with tephra from nearby Mount Takahe (24, 25) (76.28°S, 112.08°W), a recently active, flat-topped stratovolcano in West Antarctica located 360 km north of the WD coring site (Fig. 3). Therefore, we refer to the ~192-y series of volcanic eruptions as the "17.7 ka Mount Takahe Event." Estimates of emissions from Mount Takahe from enhancements in chlorine fluxes measured in the WD, Byrd, and Taylor Glacier cores, as well as radar-based evidence on the extent of the fallout plume (Fig. 3), suggest that average and peak chlorine emissions were ~100 $Gg{\cdot}y^{-1}$ and ~400 $Gg{\cdot}y^{-1}$, respectively (*SI Appendix*, *Mt. Takahe Emission Estimates*). These levels are ~10 and ~40 times higher than modern emissions estimated for Mount Erebus (23), as well as ~0.4 and ~1.6 times those reported for Mount Etna, currently the largest point source of chlorine on Earth (22). We estimate that transport of only 1% of the 17.7 ka Mount Takahe emissions to the high-latitude SH stratosphere would have yielded chlorine concentrations comparable to those responsible for modern chlorofluorocarbon-driven ozone depletion.

All of our measurements in the WD, Byrd, and Taylor Glacier (*Materials and Methods*) cores clearly indicate that the 17.7 ka

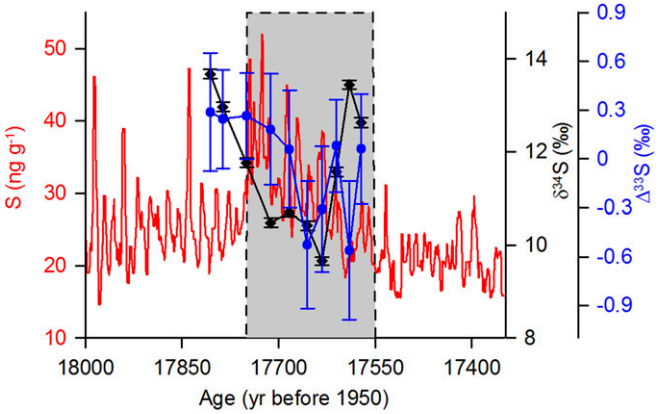

Fig. 4. Sulfur isotope anomalies indicate changes in UV radiation during the 17.7 ka event. Despite relatively modest increases in sulfur concentration in both the WD and Byrd records, volcanic sulfur emissions led to decreased $\delta^{34}S$, while increased UV radiation resulted in anomalous $\Delta^{33}S$. Uncertainties are 2σ.

event resulted from a series of massive halogen-rich, volcanic eruptions in West Antarctica (Figs. 1 and 2) (*SI Appendix*, Figs. S1–S3). Explosive volcanic eruptions inject large amounts of sulfur and other aerosols, often including halogens, into the stratosphere, frequently leading to stratospheric ozone depletion even for small eruptions (26–28) and to an increase in UV radiation at Earth's surface. Photolysis and precipitation scavenging at warmer, lower-latitude sites limit atmospheric lifetimes of volcanic halogens and thus the impacts on stratospheric ozone, although transport of even a small fraction of halogen emissions to the stratosphere can deplete ozone (29). Halogen lifetimes during the 17.7 ka event, however, were extended at Mount Takahe by the extremely cold and dry LGM conditions, particularly during dark winter months. Such a massive and persistent (~192-y) series of halogen-rich volcanic eruptions is unique within the ~68-ky WD ice core record, and the event straddles the most significant abrupt climate change recorded in Antarctic ice cores and other SH climate proxies during the >10-ky period of the last deglaciation (Figs. 1 and 2) which occurred many thousands of years after the 65°S LGM insolation minimum. The probability that these two unique events coincided by chance is the product of the two individual probabilities, and on the order of one in a million. Rather than a highly improbable coincidence, we hypothesize that these massive halogen-rich eruptions are linked causally, by stratospheric ozone depletion, to large-scale changes in SH climate and related changes in atmospheric and oceanic circulation analogous to those from modern, halogen-catalyzed ozone depletion.

Evidence for Stratospheric Ozone Depletion

Evidence for ejection of volcanic material from the 17.7 ka Mount Takahe Event into the stratosphere and/or enhanced tropospheric UV radiation was found in sulfur isotope anomalies in the WD and Byrd cores (Fig. 4). Sulfur concentrations during the ~192-y event were 1.7 times higher than background, and $\delta^{34}S$ values were lower, indicating a volcanic source of the elevated sulfur, since background marine and volcanic sources have $\delta^{34}S$ signatures of 15 to 21‰ and 0 to 5‰, respectively (30). Furthermore, exposure to UV radiation, such as when volcanic sulfur is ejected into the stratosphere above the ozone layer, generates distinct changes in sulfur isotope mass-independent fractionation (MIF; expressed as nonzero values of $\Delta^{33}S$). Previous studies have shown that MIF from a single eruption into the stratosphere follows a distinct evolution from positive to negative $\Delta^{33}S$ during the course of sulfate deposition (31), so low-resolution sampling and multiple overlapping explosive events may result in small values of $\Delta^{33}S$ even for stratospheric eruptions. The $\Delta^{33}S$ of sulfate from before the 17.7 ka event was within 2σ uncertainty of zero, as expected for nonstratospheric sulfate (31, 32). The nonzero $\Delta^{33}S$ measured in the ice during the 17.7 ka event indicated that the volcanic sulfur was indeed bombarded by enhanced UV radiation, either in the stratosphere as a result of ejection above the ozone layer and/or in the troposphere after significant stratospheric ozone depletion. The resolution of the WD and Byrd samples, the multiple explosive phases of the Mount Takahe eruptions, and the low concentration of volcanic sulfur above background levels, however, meant that the magnitude of the MIF anomaly was significant outside of 2σ only for a few samples (*Materials and Methods*).

Evidence for stratospheric ozone depletion and enhanced near-surface UV radiation also comes from changes in bromine concentration in the WD and Byrd ice core records. Photochemical reactions in near-surface snow cause rapid cycling between the snow and air for a broad range of reactive and volatile chemical species, including bromine and nitrate, and a net loss in the snow through time, known as reversible deposition (33, 34). The magnitude of this loss primarily depends on the duration and intensity of exposure of the snow to UV radiation, with duration determined by the burial rate (*SI Appendix*, *Evidence for Reversible Bromine Deposition in Antarctic Snow*), since light penetration below ~0.3 m in the snowpack is much reduced and exposure intensity is determined by the level of impinging UV radiation. During 27 ka to 6 ka in the WD record, there were only two sustained declines in bromine concentration, and the longest and most pronounced decline exactly coincided with the 17.7 ka Mount Takahe Event (Fig. 1). Annual layering in fine insoluble dust particle concentrations in the WD record indicates that the snowfall rate did not change during this period, eliminating burial rate variations as the cause of the bromine decline and implicating increased surface UV radiation (*SI Appendix*, *Snowpack Modeling*).

While bromine release from the snowpack is sensitive to changes in UV radiation, and that sensitivity increases with snow acidity (33), photochemical model simulations as well as examination of the WD record show that acidity alone is not sufficient to explain the observed bromine depletion. First, bromine concentrations in the WD and Byrd cores remained low even during periods between the nine volcanic pulses of the 17.7 ka Mount Takahe Event when concentrations of nearly all elements and chemical species, including acidity, returned to near-background concentrations (*SI Appendix*, Figs. S1 and S2). WD snow accumulation was relatively high (>100 $kg{\cdot}m^{-2}{\cdot}y^{-1}$) during this period (18), so the regions of high acidity in the core were well separated from regions of low acidity. Second, consistent with modern observations in which some but not all volcanic eruptions are associated with ozone depletion (26), evaluation of the 100 highest acidity events (annual average concentration >3.0 $\mu eq{\cdot}L^{-1}$) in the 10 ka to 25 ka WD record shows that 30% were not associated with bromine depletion and that depletion was not proportional to acidity (*SI Appendix*, Fig. S6). This clearly demonstrates that acidity alone did not lead to bromine depletion and suggests that both increased acidity and increased UV radiation were required, as predicted by modeling (*SI Appendix*, *Snowpack Modeling*).

It is unclear whether modern ozone depletion and enhanced surface UV have resulted in bromine depletion in near-surface snow. First, modern chlorofluorocarbon-driven ozone depletion largely has been confined to spring, while volcanically driven Mount Takahe ozone depletion may have persisted throughout the austral summer when the impact on snowpack photochemistry was greater. Second, there was no recent increase in acidity in Antarctic snow, so the sensitivity of bromine reemission to enhanced UV radiation was low. Third, no suitable Antarctic ice core record of bromine was available to assess the modern period (*SI Appendix*, *Comparisons to Modern Ozone Depletion*).

Plausible Linkages to Rapid SH Deglaciation

Observations and climate model simulations indicate that modern anthropogenic ozone depletion is linked to surface climate changes throughout the SH substantially similar to those ~17.7 ka, as documented in paleoclimate archives. These include a poleward shift and acceleration of the westerly winds around Antarctica (35), acceleration of midlatitude easterly winds (35), and southward expansion of the summertime Hadley cell, leading to changes in temperature and precipitation extending from the Antarctic Peninsula (36) to the subtropics, especially during austral summer (37). Specific climate changes include subtropical moistening and midlatitude drying (37) (Fig. 5), as well as pronounced warming in the northern Antarctic Peninsula and Patagonia, with cooling over the Antarctic continent, particularly in East Antarctica (35). Enhanced deep-ocean ventilation around Antarctica with reduction in oceanic uptake of CO_2 (38) also is associated with these modern changes in the westerlies. Quasi-equilibrium simulations of the potential impacts of a sustained ozone hole at 17.7 ka using a coupled Atmosphere Ocean General Circulation Model (AOGCM) initialized to LGM conditions predict qualitatively similar responses compared with the

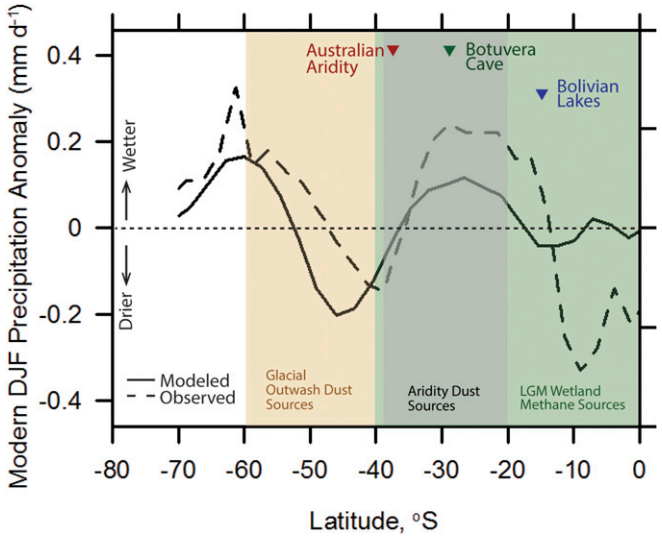

Fig. 5. Observed and modeled SH precipitation anomalies linked to modern stratospheric ozone depletion. Shown are observed and modeled zonal mean austral summer (DJF) net precipitation changes between 1979 and 2000 (37). Changes represent a ∼10% increase between 15°S and 35°S relative to the climatology (37). Simulated LGM responses to stratospheric ozone depletion are qualitatively similar (*SI Appendix, AOGCM Simulations*). Approximate latitude ranges for SH aridity and glacial outwash dust sources as well as wetlands during the LGM are indicated. Sharp changes in SH climate proxies occur exactly at this time (4, 6, 7, 10, 11, 14) (Fig. 1).

modern ozone hole. These simulations include surface warming of 0.4 °C to 0.8 °C over all of Antarctica and the Southern Ocean, in agreement with quasi-equilibrium simulations of the modern ozone hole (39, 40) (*SI Appendix, AOGCM Simulations*). These longer-term surface temperature responses are separate from the initial cooling simulated for modern stratospheric ozone depletion (41).

Previous studies (e.g., ref. 42) suggested that rising insolation initiated melting of Northern Hemisphere (NH) ice sheets at 19 ka, which triggered a reduction in the strength of the Atlantic overturning circulation, and, through the bipolar seesaw, resulted in SH warming and CO_2 release from the Southern Ocean, although the exact mechanisms driving the CO_2 release are still debated. We postulate that the ∼192-y series of halogen-rich eruptions of Mount Takahe and the subsequent ozone hole (26) initiated a series of events analogous to the modern ozone hole that acted to accelerate deglaciation at 17.7 ka. First, stratospheric ozone depletion changed SH atmospheric circulation, resulting in a rapid increase and poleward shift in the westerlies (35) (*SI Appendix*, Fig. S7). Second, consequent widespread perturbations in SH hydrometeorology, including increased austral summer subtropical precipitation between ∼15°S and ∼35°S (Figs. 1*F* and 5), led to enhanced CH_4 wetland emissions (43). Third, the combination of increased subtropical and decreased midlatitude precipitation, lower wind speeds between ∼35°S and ∼50°S (Fig. 5) (8, 37, 44), and warming centered at ∼60°S (35) (*SI Appendix*, Fig. S7), altered climate throughout SH LGM dust source regions (45). The result was a pronounced, synchronous, ∼50% decline in SH dust deposition (Fig. 1), reducing ocean biological uptake (10, 46) and thereby sharply reducing the ocean CO_2 sink. In Patagonia and New Zealand, warmer and dryer conditions south of ∼35°S (37) led to the well-documented retreat of glaciers (4–6) that starved glacial outwash plains of their fine-sediment resupply (45), with lower wind speeds possibly also contributing to reduced dustiness (47). In aridity-driven SH dust source regions located north of ∼35°S (Australia, Africa, extratropical South America), a cooler and wetter climate (37) sharply reduced aridity and hence dust export (9). Fourth, westerlies shifted poleward (*SI Appendix*, Fig. S8) and thus altered sea ice extent, leading to changes in upwelling of deep ocean carbon and nutrients, particularly in austral summer when, because of minimal sea ice and generally lower wind speeds, impacts on the carbon cycle were most pronounced (48). The net effect of these physical and biological pumps on the carbon cycle (16) likely started the release of CO_2 and initiated the rise in atmospheric CO_2 that followed the 17.7 ka Mount Takahe Event (Fig. 1) (14, 15). As with modern increases in greenhouse gases (49), the atmospheric and oceanic circulation as well as hydroclimatic changes initiated by stratospheric ozone depletion were reinforced by rising CO_2 (15) and CH_4 (12, 16).

Conclusion

Although the climate system already was primed for the switch from a glacial to interglacial state by insolation changes (1) and NH land ice loss (42), the ∼192-y ozone hole resulting from the halogen-rich eruptions of Mount Takahe plausibly provided supplementary forcing during the last termination that drove the westerly wind belt poleward and altered SH hydroclimate, providing a straightforward explanation for the synchronicity and abruptness of the SH climatic changes and global greenhouse gases that occurred ∼17.7 ka.

Materials and Methods

Ice Core Measurements. A nearly contiguous set of longitudinal WD samples from 1,300 m to 2,710 m depth was analyzed using a state-of-the-art continuous ice core analytical system (50–53) (*SI Appendix*, Fig. S8), in addition to replicate WD samples from 2,419.3 m to 2,435.2 m and all samples of the Byrd core (17) available from the University of Copenhagen archive between 1,242.06 ma and 1,303.39 m depth (*SI Appendix, Continuous Ice Core Measurements*). Samples from Taylor Glacier in the Antarctic Dry Valleys (54) also provided a record of the Mount Takahe event (Fig. 3). Additional measurements, including fluoride, bromide, and methane sulfonic acid, were made on discrete samples (*SI Appendix, Discrete Ice Core Measurements*).

Sulfur isotopes were measured on selected discrete samples using multicollector inductively coupled plasma mass spectrometry (ICP-MS) (55). The measured isotopic ratios were converted to δ values (Vienna-Canyon Diablo Troilite) using the International Atomic Energy Agency standards S5 and S6 and the standard NBS127. The $\delta^{34}S$ and $\delta^{33}S$ values of $NaSO_4$ ($\Delta^{33}S = 0$) were used to calibrate the instrument. The instrumental uncertainty for $\Delta^{33}S$, defined as 2 times the SD (2σ) of replicate measurement of the internal standards, was ±0.42‰. Volcanic events in ice cores previously sampled for sulfur isotope studies contained volcanic sulfur concentrations typically 3- to 10-fold greater than background sulfur concentrations (31, 32). Sulfur concentrations during the 17.7 ka event were only 1.7 times background (Fig. 4).

In a reinterpretation of the original Byrd core measurements (17), LaViolette (21) proposed an extraterrestrial origin. Helium (He), and especially ^3He, is much higher in extraterrestrial matter than in terrestrial components (56). Approximately 3 kg of discrete meltwater samples were collected from the outer ring of the melter head for He concentration and isotope measurements above, within, and below the 17.7 ka event. Average ^3He concentrations were 4.4e-17 (±2.5e-17) $cm^3 \cdot g^{-1}$ and 3.7e-17 (±2.5e-17) $cm^3 \cdot g^{-1}$ in the five background and four 17.7 ka event samples, respectively. Similarly, the $^3He/^4He$ ratios were 6.8e-5 (±1.7e-5) in the background samples and 7.3e-5 (±1.9e-5) in the event samples. Interplanetary dust fluxes calculated from these data were in agreement with past measurements (57), indicating no evidence for an extraterrestrial source for the 17.7 ka anomaly.

Volcanic Tephra Measurements. Insoluble tephra particles were captured on 10-μm stainless steel filters during continuous analyses for a background section of WD ice with no chemical evidence of volcanic fallout, as well as two sets of filters representing the early and later stages during the extended volcanic period (*SI Appendix*, Fig. S8). Additional tephra was filtered from larger-volume, discrete samples collected as part of targeted replicate coring at WD (*SI Appendix, Tephra Sampling and Geochemistry*).

Small concentrations of silicate particles were detected for the depth interval corresponding to the early stages of the 17.7 ka event (2,430 m to 2,426 m). No glass shards were found in the background sample or in the sample corresponding to the later stages of the 17.7 ka event, consistent with the continuous

insoluble particle measurements (*SI Appendix*, Fig. S1). Most of the particles identified in the sample were fine (~10 μm), and some had cuspate shapes suggestive of volcanic origin. Quantitative geochemical analysis of the particles indicates the presence of volcanic glass with an iron-rich trachytic composition characteristic of West Antarctic volcanism (*SI Appendix*, Table S1). The two main eruptive source volcanoes in West Antarctica, Mount Takahe (76°18.8′S, 112°4.8′W) and Mount Berlin (76°3′S, 136°0′W), are located 350 km north and 670 km northwest of the WD drilling site, respectively. The composition of tephra erupted from these two volcanoes is similar but can be distinguished by examining the MgO content of the volcanic glass, which is significantly higher in Mount Takahe eruptions (up to 0.5 wt.%) than in Mount Berlin eruptions, many of which have undetectable levels of MgO (24, 58).

Break Point Estimates. The break function regression algorithm BREAKFIT (59) was used to estimate the timing and uncertainty (1σ) of concentration changes in nssCa, CH_4, and CO_2 (Fig. 2). Intersecting linear trends were fit to nssCa and CH_4 measurements corresponding to 17.0 ka to 20.0 ka, and CO_2 measurements corresponding to 16.0 ka to 20.0 ka. Estimated break points for nssCa and CH_4 were 17.882 ka (±0.179 ka) and 17.759 ka (±0.075 ka), respectively. Similarly, the break point for CO_2 was 17.612 ka (±0.051 ka).

ACKNOWLEDGMENTS. We acknowledge R. von Glasow for help with snowpack model simulations, and J. Stutz and R. Kreidberg for helpful discussions. The US National Science Foundation supported this work [Grants 0538427, 0839093, and 1142166 (to J.R.M.); 1043518 (to E.J.B.); 0538657 and 1043421 (to J.P. Severinghaus); 0538553 and 0839066 (to J.C.-D.); and 0944348, 0944191, 0440817, 0440819, and 0230396 (to K.C.T.)]. We thank the WAIS Divide Science Coordination Office and other support organizations. P.K. and G.K. were funded by Polar Regions and Coasts in a Changing Earth System-II, with additional support from the Helmholtz Climate Initiative.

1. Hays JD, Imbrie J, Shackleton NJ (1976) Variations in Earth's orbit - Pacemaker of ice ages. *Science* 194:1121–1132.
2. Cheng H, et al. (2009) Ice age terminations. *Science* 326:248–252.
3. Landais A, et al. (2013) Two-phase change in CO_2, Antarctic temperature and global climate during Termination II. *Nat Geosci* 6:1062–1065.
4. Boex J, et al. (2013) Rapid thinning of the late Pleistocene Patagonian Ice Sheet followed migration of the Southern Westerlies. *Sci Rep* 3:2118.
5. Moreno P, et al. (2015) Radiocarbon chronology of the Last Glacial Maximum and its termination in northwestern Patagonia. *Quat Sci Rev* 122:233–249.
6. Putnam A, et al. (2013) Warming and glacier recession in the Rakaia valley, Southern Alps of New Zealand, during Heinrich Stadial 1. *Earth Planet Sci Lett* 382:98–110.
7. Placzek C, Quade J, Patchett PJ (2006) Geochronology and stratigraphy of late Pleistocene lake cycles on the southern Bolivian Altiplano: Implications for causes of tropical climate change. *Geol Soc Am Bull* 118:515–532.
8. Cruz FW, Jr, et al. (2005) Insolation-driven changes in atmospheric circulation over the past 116,000 years in subtropical Brazil. *Nature* 434:63–66.
9. De Deckker P, Moros M, Perner K, Jansen E (2012) Influence of the tropics and southern westerlies on glacial interhemispheric asymmetry. *Nat Geosci* 5:266–269.
10. Martínez-García A, et al. (2014) Iron fertilization of the Subantarctic ocean during the last ice age. *Science* 343:1347–1350.
11. Lambert F, et al. (2008) Dust-climate couplings over the past 800,000 years from the EPICA Dome C ice core. *Nature* 452:616–619.
12. WAIS Divide Project Members (2013) Onset of deglacial warming in West Antarctica driven by local orbital forcing. *Nature* 500:440–444.
13. Cuffey KM, et al. (2016) Deglacial temperature history of West Antarctica. *Proc Natl Acad Sci USA* 113:14249–14254.
14. Schmitt J, et al. (2012) Carbon isotope constraints on the deglacial CO_2 rise from ice cores. *Science* 336:711–714.
15. Marcott SA, et al. (2014) Centennial-scale changes in the global carbon cycle during the last deglaciation. *Nature* 514:616–619.
16. Völker C, Köhler P (2013) Responses of ocean circulation and carbon cycle to changes in the position of the Southern Hemisphere westerlies at Last Glacial Maximum. *Paleoceanography* 28:726–739.
17. Hammer CU, Clausen HB, Langway CC (1997) 50,000 years of recorded global volcanism. *Clim Change* 35:1–15.
18. Sigl M, et al. (2016) The WAIS Divide deep ice core WD2014 chronology - Part 2: Annual-layer counting (0-31 ka BP). *Clim Past* 12:769–786.
19. Neumann TA, et al. (2008) Holocene accumulation and ice sheet dynamics in central West Antarctica. *J Geophys Res Earth Surf* 113:9.
20. Matsumoto A, Hinkley TK (2001) Trace metal suites in Antarctic pre-industrial ice are consistent with emissions from quiescent degassing of volcanoes worldwide. *Earth Planet Sci Lett* 186:33–43.
21. LaViolette PA (2005) Solar cycle variations in ice acidity at the end of the last ice age: Possible marker of a climatically significant interstellar dust incursion. *Planet Space Sci* 53:385–393.
22. Francis P, Burton MR, Oppenheimer C (1998) Remote measurements of volcanic gas compositions by solar occultation spectroscopy. *Nature* 396:567–570.
23. Wardell LJ, Kyle PR, Counce D (2008) Volcanic emissions of metals and halogens from White Island (New Zealand) and Erebus volcano (Antarctica) determined with chemical traps. *J Volcanol Geotherm Res* 177:734–742.
24. Wilch TI, McIntosh WC, Dunbar NW (1999) Late Quaternary volcanic activity in Marie Byrd Land: Potential Ar-40/Ar-39-dated time horizons in West Antarctic ice and marine cores. *Geol Soc Am Bull* 111:1563–1580.
25. Palais JM, Kyle PR, McIntosh WC, Seward D (1988) Magmatic and phreatomagmatic volcanic activity at Mt Takahe, West Antarctica, based on tephra layers in the Byrd ice core and field observations at Mt Takahe. *J Volcanol Geotherm Res* 35:295–317.
26. Kutterolf S, et al. (2013) Combined bromine and chlorine release from large explosive volcanic eruptions: A threat to stratospheric ozone? *Geology* 41:707–710.
27. Solomon S, et al. (2016) Emergence of healing in the Antarctic ozone layer. *Science* 353:269–274.
28. Ivy D, et al. (2017) Observed changes in the Southern Hemispheric circulation in May. *J Clim* 30:527–536.
29. Cadoux A, Scaillet B, Bekki S, Oppenheimer C, Druitt TH (2015) Stratospheric ozone destruction by the Bronze-Age Minoan eruption (Santorini Volcano, Greece). *Sci Rep* 5:12243.
30. Patris N, Delmas RJ, Jouzel J (2000) Isotopic signatures of sulfur in shallow Antarctic ice cores. *J Geophys Res Atmos* 105:7071–7078.
31. Baroni M, Thiemens MH, Delmas RJ, Savarino J (2007) Mass-independent sulfur isotopic compositions in stratospheric volcanic eruptions. *Science* 315:84–87.
32. Savarino J, Romero A, Cole-Dai J, Thiemens MH (2003) UV induced mass-independent sulfur composition in stratospheric volcanic eruptions. *Geochim Cosmochim Acta* 67: A417–A417.
33. Abbatt JPD, et al. (2012) Halogen activation via interactions with environmental ice and snow in the polar lower troposphere and other regions. *Atmos Chem Phys* 12: 6237–6271.
34. Thomas JL, et al. (2011) Modeling chemistry in and above snow at Summit, Greenland - Part 1: Model description and results. *Atmos Chem Phys* 11:4899–4914.
35. Thompson DWJ, et al. (2011) Signatures of the Antarctic ozone hole in Southern Hemisphere surface climate change. *Nat Geosci* 4:741–749.
36. Polvani LM, Waugh DW, Correa GJP, Son S-W (2011) Stratospheric ozone depletion: The main driver of twentieth-century atmospheric circulation changes in the Southern Hemisphere. *J Clim* 24:795–812.
37. Kang SM, Polvani LM, Fyfe JC, Sigmond M (2011) Impact of polar ozone depletion on subtropical precipitation. *Science* 332:951–954.
38. Waugh DW, Primeau F, Devries T, Holzer M (2013) Recent changes in the ventilation of the southern oceans. *Science* 339:568–570.
39. Bitz CM, Polvani LM (2012) Antarctic climate response to stratospheric ozone depletion in a fine resolution ocean climate model. *Geophys Res Lett* 39:L20705.
40. Ferreira D, Marshall J, Bitz C, Solomon S, Plumb A (2015) Antarctic Ocean and sea ice response to ozone depletion: A two-time-scale problem. *J Clim* 28:1206–1226.
41. Solomon A, Polvani L, Smith K, Abernathey R (2015) The impact of ozone depleting substances on the circulation, temperature, and salinity of the Southern Ocean: An attribution study with CESM1(WACCM). *Geophys Res Lett* 42:5547–5555.
42. Shakun JD, et al. (2012) Global warming preceded by increasing carbon dioxide concentrations during the last deglaciation. *Nature* 484:49–54.
43. Baumgartner M, et al. (2012) High-resolution interpolar difference of atmospheric methane around the Last Glacial Maximum. *Biogeosciences* 9:3961–3977.
44. Gonzalez PM, Polvani L, Seager R, Correa GP (2013) Stratospheric ozone depletion: A key driver of recent precipitation trends in South Eastern South America. *Clim Dyn* 42: 1775–1792.
45. Sugden DE, McCulloch RD, Bory AJM, Hein AS (2009) Influence of Patagonian glaciers on Antarctic dust deposition during the last glacial period. *Nat Geosci* 2:281–285.
46. Bauska TK, et al. (2016) Carbon isotopes characterize rapid changes in atmospheric carbon dioxide during the last deglaciation. *Proc Natl Acad Sci USA* 113:3465–3470.
47. Mcgee D, Broecker W, Winckler G (2010) Gustiness: The driver of glacial dustiness? *Quat Sci Rev* 29:2340–2350.
48. Hauck J, et al. (2013) Seasonally different carbon flux changes in the Southern Ocean in response to the southern annular mode. *Global Biogeochem Cycles* 27:1236–1245.
49. Son SW, et al. (2008) The impact of stratospheric ozone recovery on the Southern Hemisphere westerly jet. *Science* 320:1486–1489.
50. McConnell JR, et al. (2014) Antarctic-wide array of high-resolution ice core records reveals pervasive lead pollution began in 1889 and persists today. *Sci Rep* 4:5848.
51. Sigl M, et al. (2015) Timing and climate forcing of volcanic eruptions for the past 2,500 years. *Nature* 523:543–549.
52. Maselli OJ, et al. (2017) Sea ice and pollution-modulated changes in Greenland ice core methanesulfonate and bromine. *Clim Past* 13:39–59.
53. McConnell JR, Edwards R (2008) Coal burning leaves toxic heavy metal legacy in the Arctic. *Proc Natl Acad Sci USA* 105:12140–12144.
54. Baggenstos D (2015) Taylor Glacier as an archive of ancient ice for large-volume samples: Chronology, gases, dust, and climate. PhD thesis (Univ Calif, San Diego).
55. Paris G, Sessions AL, Subhas AV, Adkins JF (2013) MC-ICP-MS measurement of delta S-34 and Delta S-33 in small amounts of dissolved sulfate. *Chem Geol* 345:50–61.
56. Farley KA, Mukhopadhyay S (2001) An extraterrestrial impact at the Permian-Triassic boundary? *Science* 293:2343.
57. Winckler G, Fischer H (2006) 30,000 years of cosmic dust in Antarctic ice. *Science* 313:491.
58. Dunbar NW, McIntosh WC, Esser RP (2008) Physical setting and tephrochronology of the summit caldera ice record at Mount Moulton, West Antarctica. *Geol Soc Am Bull* 120:796–812.
59. Mudelsee M (2009) Break function regression. *Eur Phys J Spec Top* 174:49–63.
60. Rhodes RH, et al. (2015) Paleoclimate. Enhanced tropical methane production in response to iceberg discharge in the North Atlantic. *Science* 348:1016–1019.

`

Supporting Information Appendix

Synchronous volcanic eruptions and abrupt climate change ~17.7k years ago plausibly linked by stratospheric ozone depletion

Joseph R. McConnell, Andrea Burke, Nelia W. Dunbar, Peter Köhler, Jennie L. Thomas, Monica M. Arienzo, Nathan J. Chellman, Olivia J. Maselli, Michael Sigl, Jess F. Adkins, Daniel Baggenstos, John F. Burkhart, Edward J. Brook, Christo Buizert, Jihong Cole-Dai, T.J. Fudge, Gregor Knorr, Hans-F. Graf, Mackenzie M. Grieman, Nels Iverson, Kenneth C. McGwire, Robert Mulvaney, Guillaume Paris, Rachael H. Rhodes, Eric S. Saltzman, Jeffrey P. Severinghaus, Jørgen-Peder Steffensen, Kendrick C. Taylor, Gisela Winckler

Contents

`

Continuous Ice Core Measurements

Longitudinal WD samples from ~1300 m to ~2710 m depth were analyzed for a broad range of elements and chemical species using a state-of-the-art continuous ice core analytical system (SI Appendix, Fig. S8), in addition to replicate WD samples from 2419.3 m to 2435.2 m and all samples of the Byrd core between 1242.06 to 1303.39 m depth available from the University of Copenhagen archive. The 3404 m long WD ice core (79.481^{o}S, 112.112^{o}W, 1766 m elevation) was collected from a cold (mean annual temperature -31^{o} C), high snowfall (196 kg m^{-2} y^{-1}) West Antarctic site (3). Because the core also was measured with high-resolution analytical techniques, WD provides the highest temporal resolution Antarctic climate record available for the last glacial to interglacial transition. The WD record exceeds the temporal resolution of the deep Greenland cores – GISP2, GRIP, NGRIP, NEEM – and includes a much broader range of aerosol-linked elemental and chemical tracers. The Byrd core was collected in 1968 from a site (80.02^{o}S, 119.52^{o}W) located 159 km from WD and ~200 m lower in elevation (4). Similar continuous analyses of ice samples from Taylor Glacier in the Antarctic Dry Valleys (5) provided an additional record of the 17.7ka Mt. Takahe event (Fig. 3).

Analyses were conducted on longitudinal samples (~100 mm by ~33 mm by ~33 mm) using the Desert Research Institute's well-established, continuous-flow analysis with trace elements and black carbon analytical system (6-12), recently expanded to include continuous measurements of mineral acidity (13) and CH_4 (14). The analytical system included two Element2 (Thermo Scientific) high-resolution inductively coupled plasma mass spectrometers (HR-ICP-MS) operating in parallel for measurement of a broad range of ~35 elements, an SP2 (Droplet Measurement Technologies) inter-cavity-laser-based instrument for black carbon (BC) measurements, and a number of fluorimeters and spectrophotometers for measurement of ammonium, nitrate, hydrogen peroxide, and other chemical species (SI Appendix, Fig. S8). All measurements were exactly co-registered in depth. While effective measurement resolution differed between sample streams and instruments, resolution typically was less than 10 mm for aerosol-related elements and chemical species.

Comparisons of replicate measurements from within the WD core (SI Appendix, Fig. S1) and between the WD and Byrd ice cores (SI Appendix, Fig. S2) indicate that results were highly repeatable for nearly all elements, despite the extremely low concentration levels (as low as 20 fg g^{-1}) for elements such as the low-boiling-point heavy metals (bismuth, cadmium, and thallium) and REE (lanthanum, cerium, and europium), and despite the distance between the WD and Byrd coring sites. Note the near-perfect replication of the observed bromine depletion during the 17.7ka anomaly. Under recovery of more recalcitrant elements such as Al and Fe contained in larger insoluble dust particles is implicit in continuous methods (11, 15) but does not impact measurements of heavy metals or other elements associated with gaseous volcanic emissions that generally coat the outside of insoluble particles because of the addition of ultra-pure nitric acid to the sample flow stream immediately after the melter head.

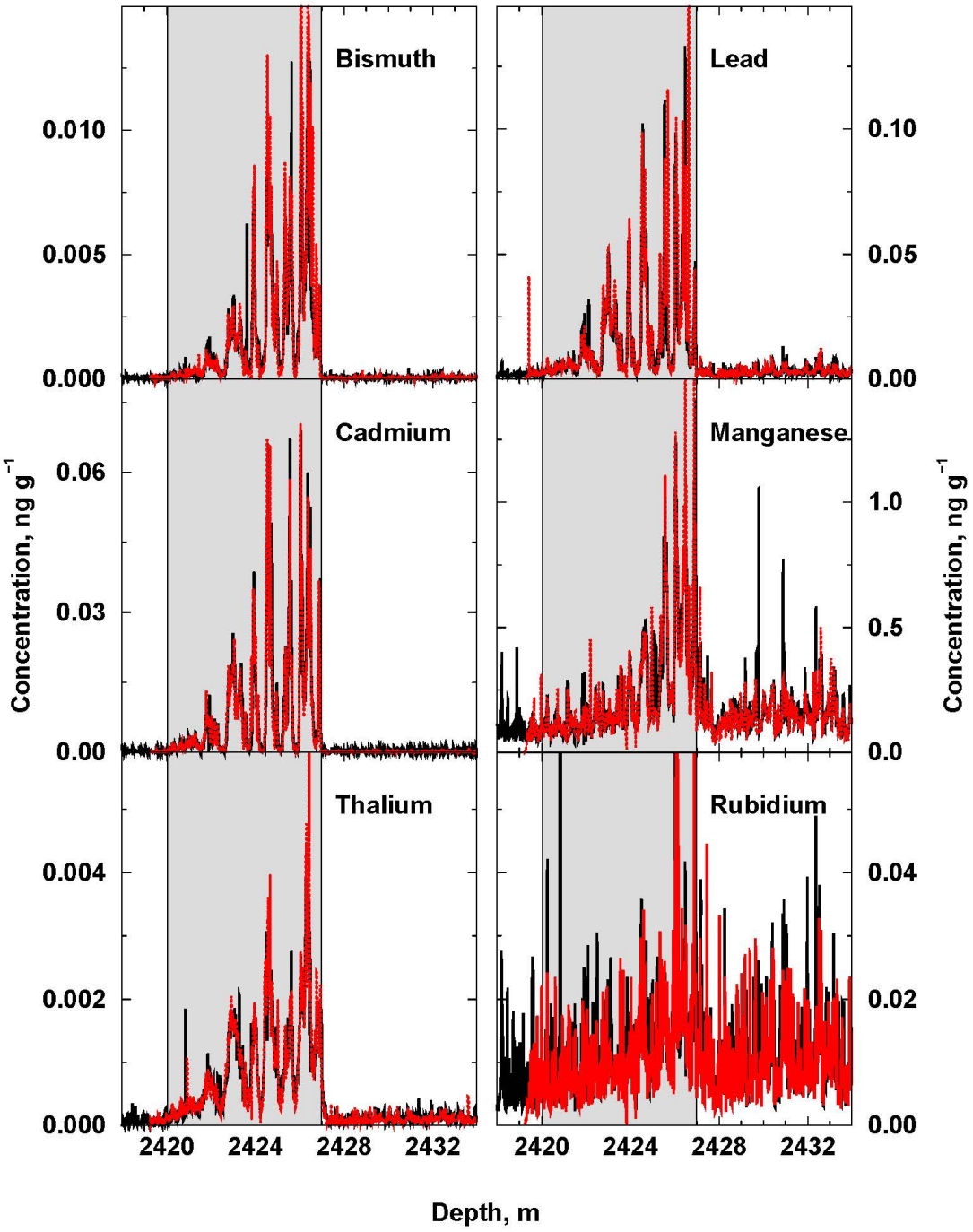

Fig. S1a-d Continuous, high-resolution measurements of selected elements and insoluble particle counts (PC) in the WAIS Divide (WD) ice core. The shaded box identifies the period of the 17.7ka anomaly in WD. Size-specific dust concentrations were calculated from insoluble particle counts. Comparison of original (black) and replicate (red) measurements on a second set of longitudinal samples shows that the measurements are highly repeatable despite the extremely low concentrations and high variability of many elements (Dataset S1).

`

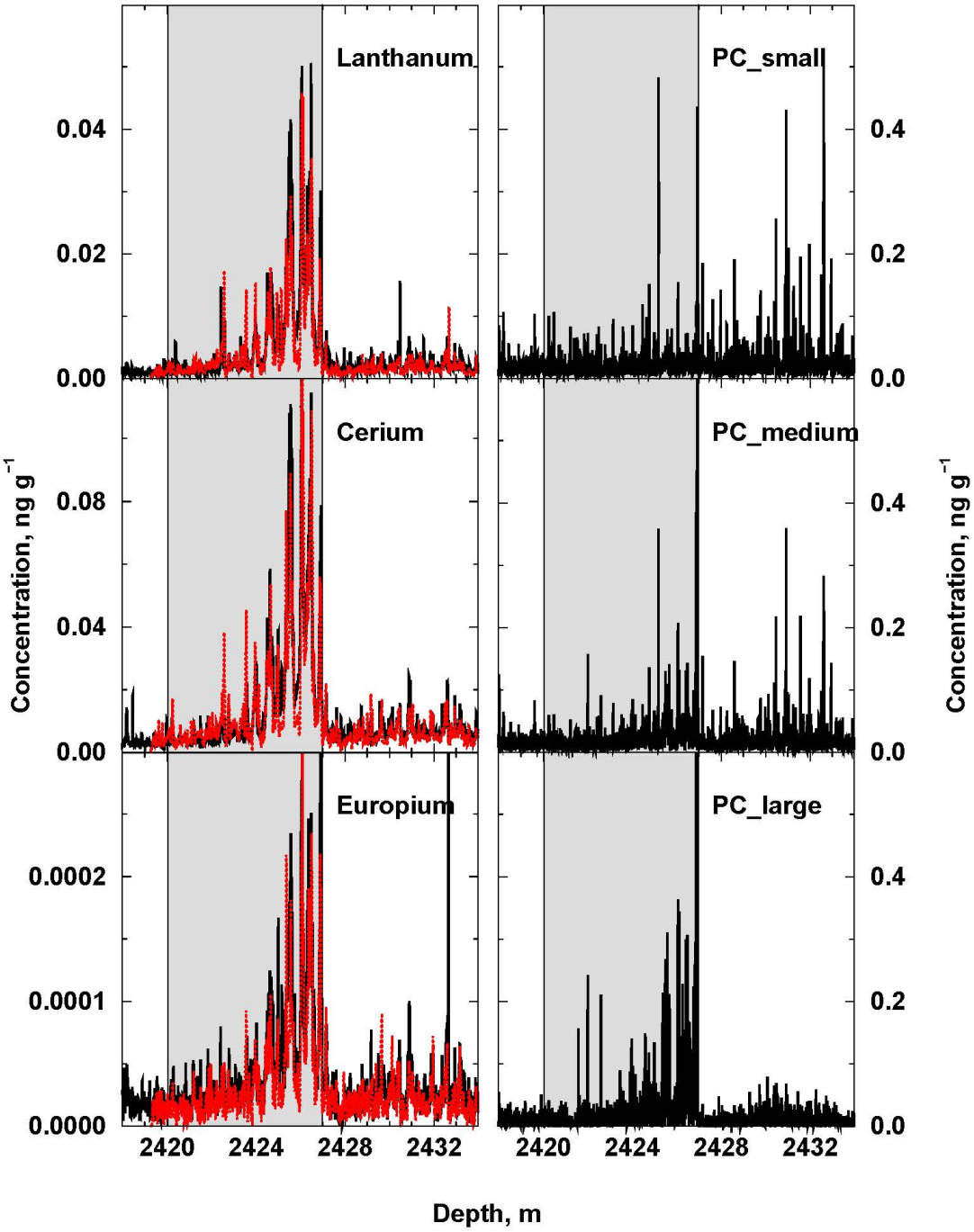
Lanthanum
Cerium
Europium
PC_small
PC_medium
PC_large
Concentration, ng g^{-1}
Concentration, ng g^{-1}
0.04
0.02
0.00
0.08
0.04
0.00
0.0002
0.0001
0.0000
0.4
0.2
0.0
0.4
0.2
0.0
0.4
0.2
0.0
2420
2424
2428
2432
2420
2424
2428
2432
Depth, m

Fig. S1b

`

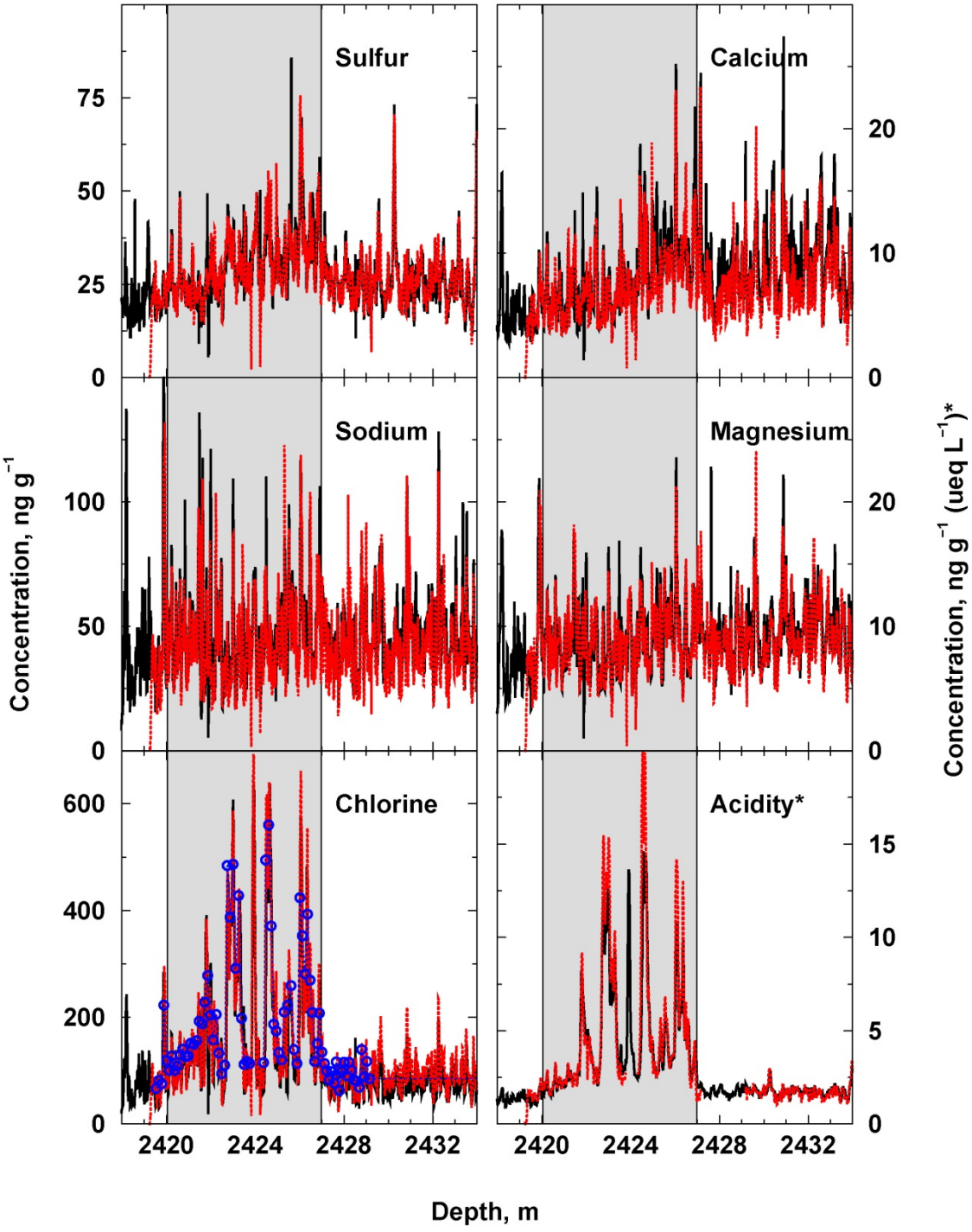
Sulfur
Calcium
Sodium
Magnesium
Chlorine
Acidity*
Concentration, ng g^{-1}
Concentration, ng g^{-1} (ueq L^{-1})*
Depth, m
0
25
50
75
100
200
400
600
5
10
15
20
2420
2424
2428
2432

Fig. S1c

`

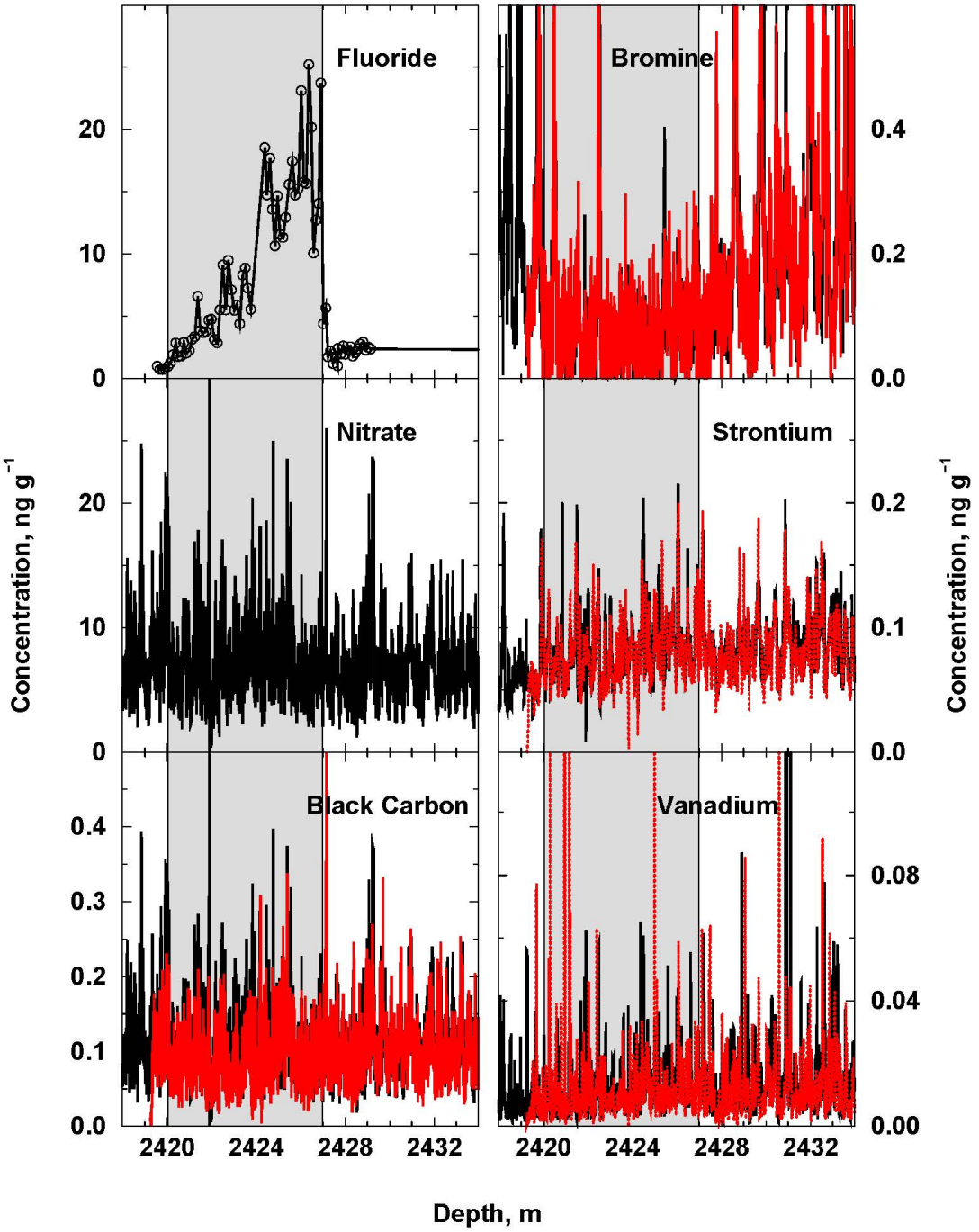
Fluoride
Bromine
Nitrate
Strontium
Black Carbon
Vanadium
Concentration, ng g^{-1}
Concentration, ng g^{-1}
Depth, m
2420
2424
2428
2432

Fig. S1d

`

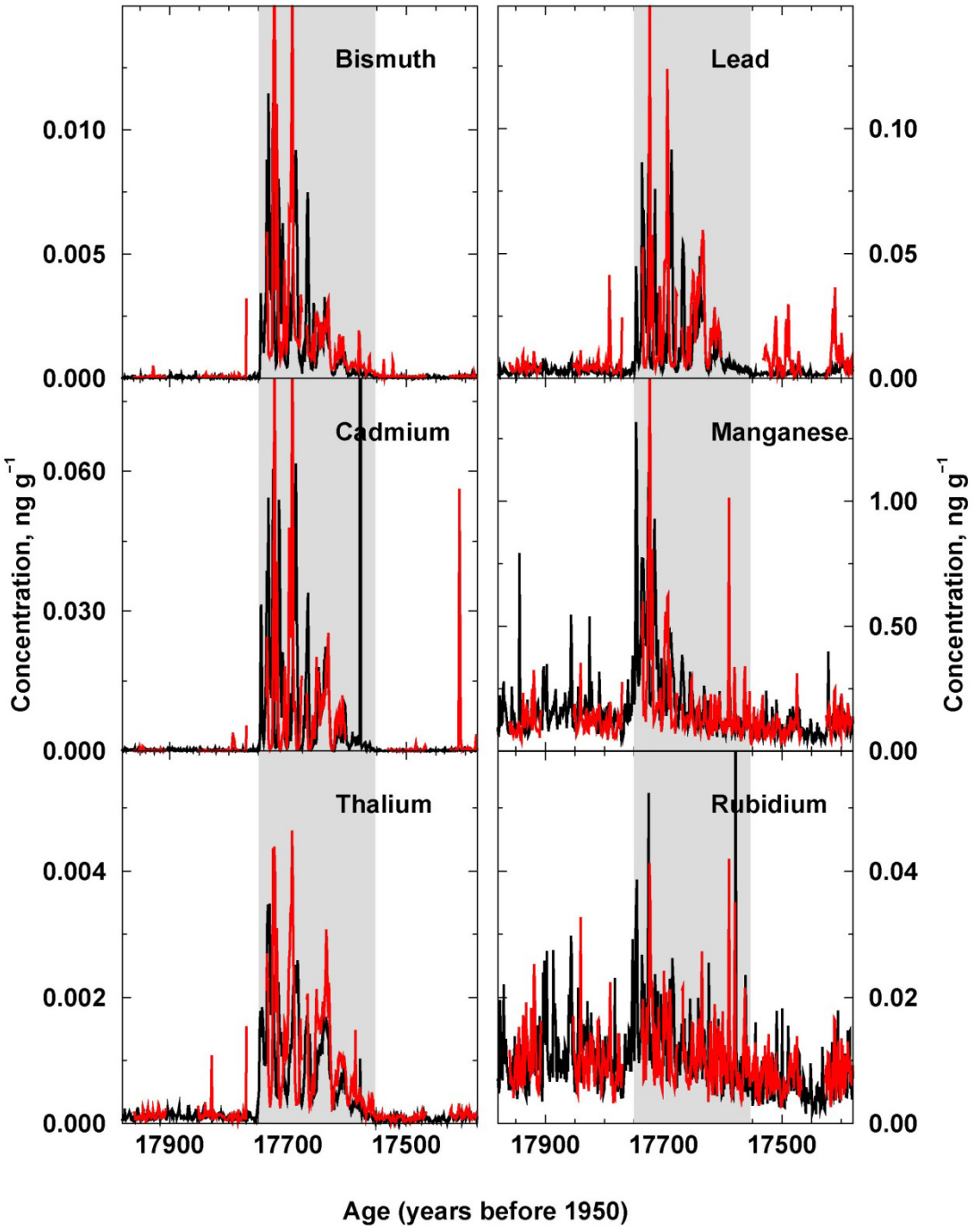

Fig. S2a-c Comparison of continuous, high-resolution measurements of selected elements in the Byrd and WD ice cores. WD measurements (black) are shown on the WD2014 timescale. The shaded box identifies the period of the 17.7ka anomaly in WD. Byrd (4) measurements (red) were made on all available samples from the University of Copenhagen archive and synchronized to WD using 20 volcanic markers between 1241 and 1295 m depth in the Byrd core. Note the very close agreement in the WD and Byrd records for all parameters despite the nearly 50-year storage time, limited contiguity of available samples from Byrd, and 159 km distance between the sites (Dataset S1).

`

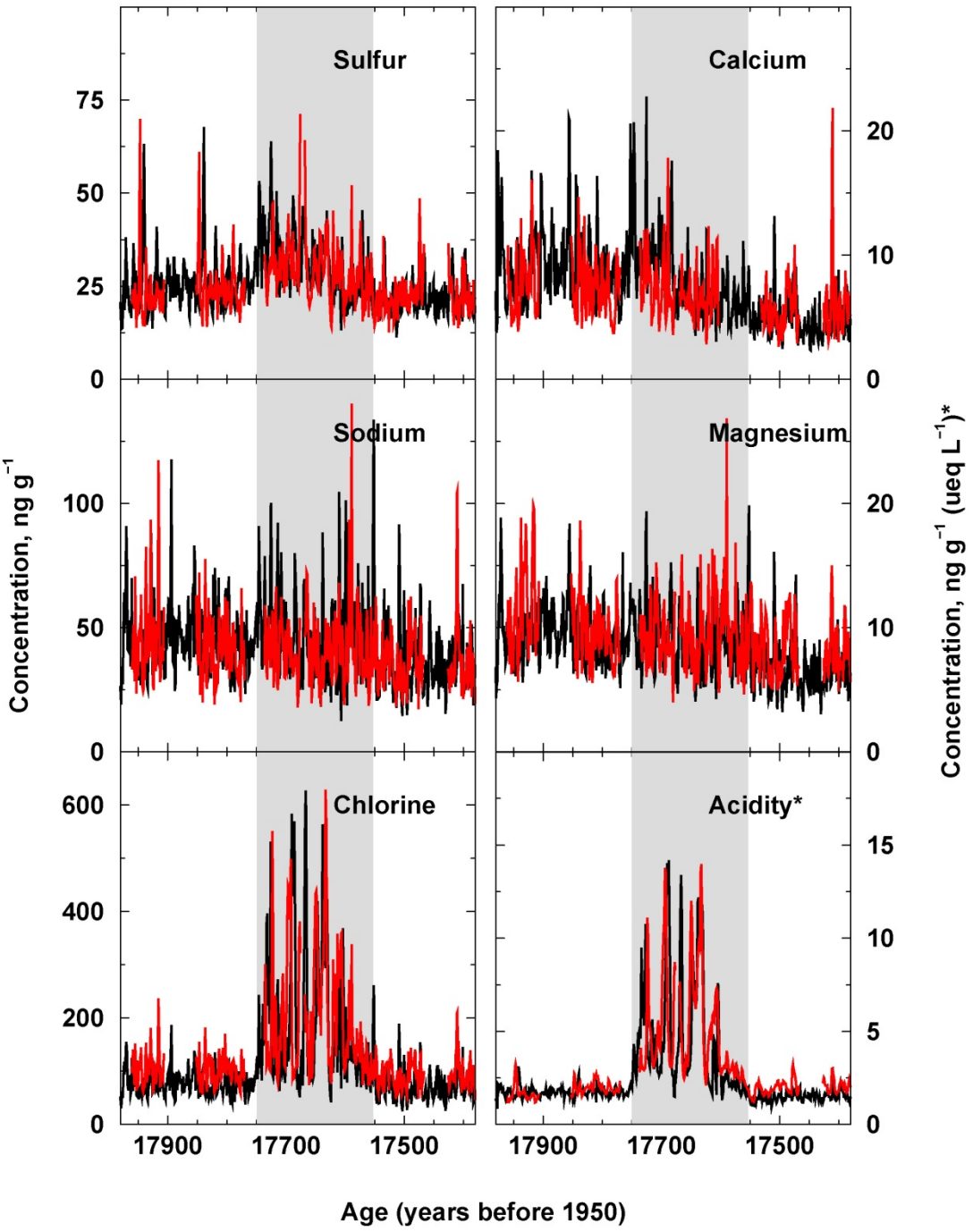
Sulfur
Calcium
Sodium
Magnesium
Chlorine
Acidity*
Concentration, ng g^{-1}
Concentration, ng g^{-1} (ueq L^{-1})*
Age (years before 1950)
17900
17700
17500

Fig. S2b

`

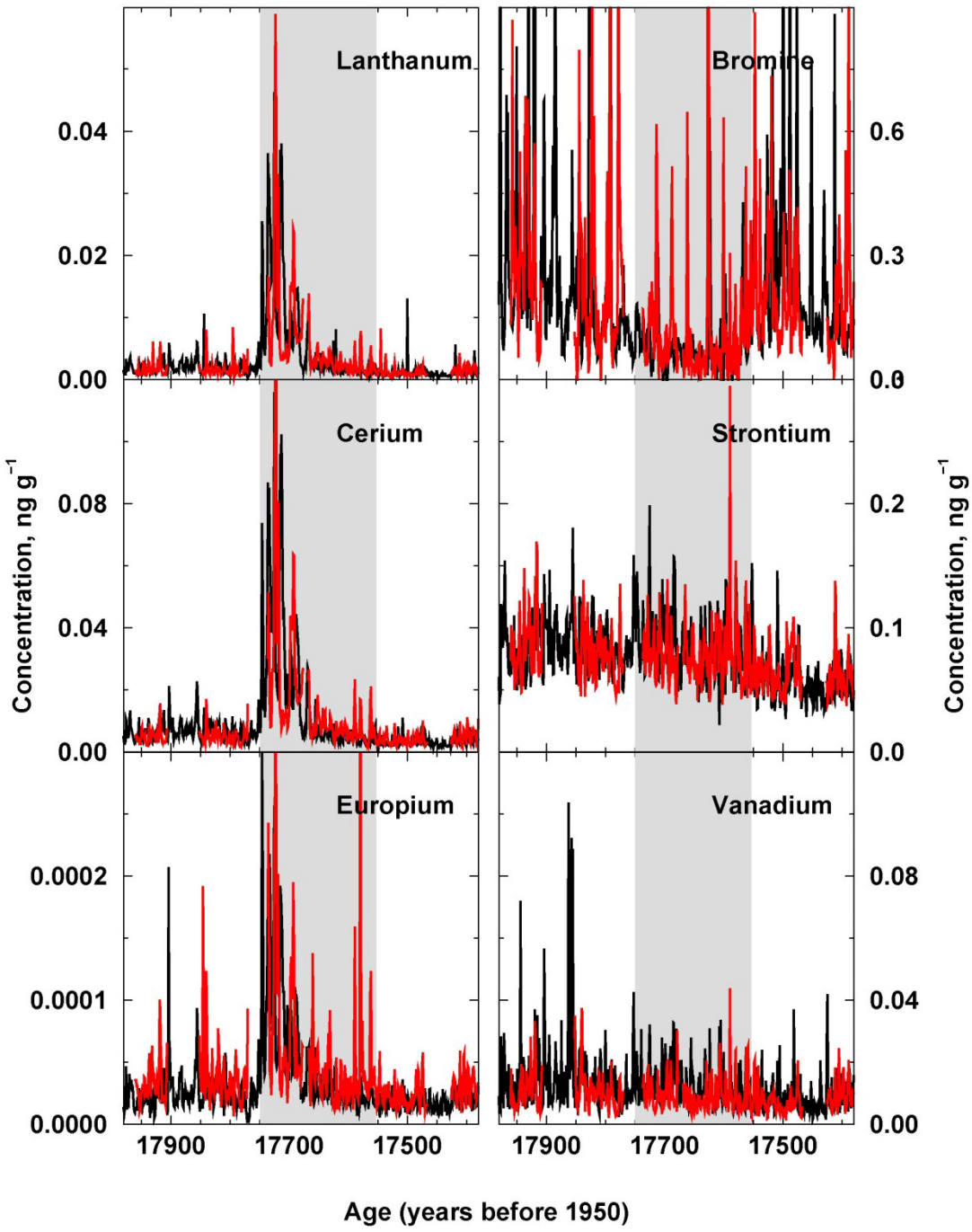
Lanthanum
Bromine
Cerium
Strontium
Europium
Vanadium
0.04
0.02
0.00
0.6
0.3
0.0
0.08
0.04
0.00
0.2
0.1
0.0
0.0002
0.0001
0.0000
0.08
0.04
0.00
17900
17700
17500
Concentration, ng g-1
Age (years before 1950)

Fig. S2c

`

Discrete Ice Core Measurements

Fluoride, bromide, and some other compounds cannot be measured with the on-line system so discrete samples were captured using a fraction collector during continuous analysis of the primary, replicate, and Byrd samples. Discrete samples were analyzed for fluoride, chloride, sulfate, and methane sulfonic acid (MSA) using ion chromatography (IC), as well as bromide and MSA using anion chromatography with detection by electrospray ionization and negative ion tandem mass spectrometry. Comparisons between the continuous ICP-MS measurements of chlorine and the discrete IC measurements of chloride show that the results are similar (SI Appendix, Fig. S3) and a pronounced depletion at 17.7ka was observed in both discrete bromide and continuous (16) bromine concentrations (SI Appendix – Bromine and Bromide).

Sulfur isotopes were measured on selected discrete samples using multi-collector ICP-MS (17).

Approximately 3 kg discrete meltwater samples were collected from the outer ring of the melter head for He concentration and isotope measurements above, within, and below the 17.7ka event. Average ^{3}He concentrations were 4.4e-17 (±2.5e-17) cm^3 g^{-1} and 3.7e-17 (±2.5e-17) cm^3 g^{-1} in the five background and four 17.7ka event samples, respectively. Similarly, the $^{3}He/^{4}He$ ratios were 6.8e-5 (±1.7e-5) in the background samples and 7.3e-5 (±1.9e-5) in the event samples.

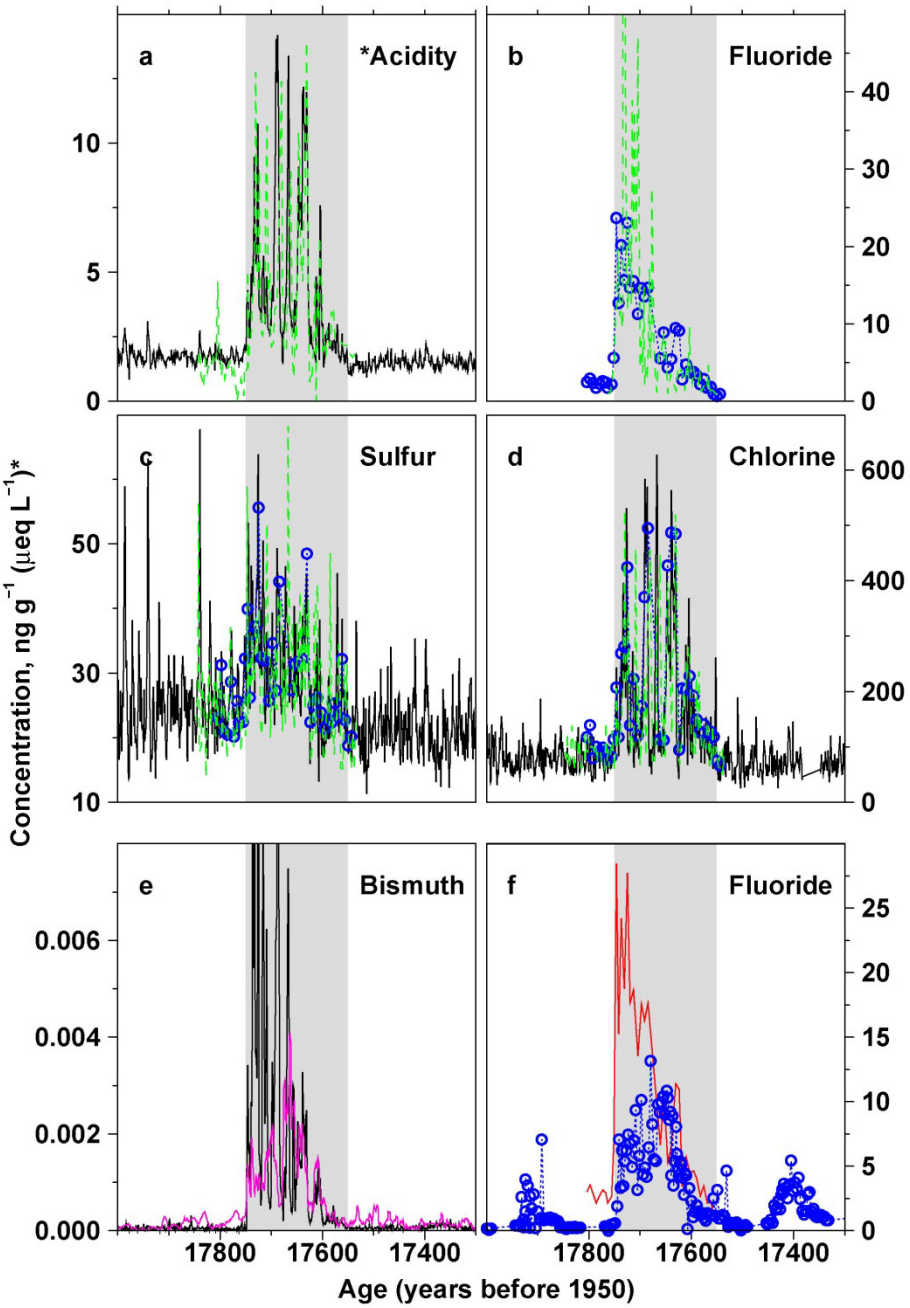

Fig. S3 Measurements showing the spatial extent of the ~17.7ka glaciochemical anomaly. (a-d): Measurements of acidity, sulfur (sulfate), and the halogens chlorine (chloride) and fluoride in the WD ice core and original (4) measurements from the Byrd ice core. Byrd measurements are shown in green (dashed line). Original continuous measurements on the WD core (Dataset S1) are shown in black with ion chromatography measurements on WD discrete samples (Dataset S1) shown in blue (circles). All the Byrd measurements are shown on the original timescale but shifted in age by 230 years to align with WD. (**e):** Bismuth measured in the WD and Taylor Glacier (magenta) cores (Dataset S1). (**f):** Fluoride measured in the WD and EDC cores (Dataset S1). The shaded boxes in **a-f** identify the period of the 17.7ka anomaly in WD.

`

Bromine and Bromide

Although often close to detection limits when measured using ion chromatography, bromide (Br^-) rarely has been measured in ice cores previously. It has been studied extensively, however, in near-surface polar snow because bromine plays an important role in snowpack photochemistry (18-20). Here we measured both total bromine (Br_{total}) and Br^- concentrations in the WD core. Good agreement was found between Br_{total} and Br^- concentrations in samples corresponding to the 17.7ka Mt. Takahe event, with both showing nearly complete depletion during the volcanic event (Fig. 1).

Br_{total} was measured continuously in the WD and Byrd cores using methods described in Maselli et al. (16). Br^- was measured in discrete samples from WD obtained using a fraction collector from the DRI continuous melter (SI Appendix, Fig. S8). Note that the discrete samples were collected from a different part of the ice core cross section than the continuous sample melt stream. The discrete samples were analyzed using anion chromatography with detection by electrospray ionization and negative ion tandem mass spectrometry (ESI/MS/MS; Thermofinnigan Quantum). The chromatography used a 1 ml injection loop, and a 2 x 150 mm AS 18 fast anion column with 0.04 M KOH eluent at a flow rate of 200 ul/min (Dionex ICS-2100 ion chromatograph). The eluent stream was mixed with 0.07 µl/min of methanol prior to entering the electrospray ion source. Bromide was detected as $^{79}Br^-$ and quantified using gravimetrically calibrated aqueous NaBr standards. The bromide signal at mass 81 also was monitored to verify the identity of the bromide peak using the bromine 79/81 isotopic ratio.

`

Tephra Sampling and Geochemistry

Continuous measurements showing high concentrations of REE, manganese, and other elements (SI Appendix, Fig. S1) found in tephra, as well as modest but clear increases in insoluble particles in the 2.5 to 10 μm range during the early stages of the 17.7ka event, indicated that tephra particles were present. During replicate continuous analyses of the main WD core, 10 μm, stainless-steel, in-line filters were added to the two lines coming from the middle ring of the melter head (SI Appendix, Fig. S8) to capture volcanic tephra particles present in the meltwater stream. Sets of filters were collected for a background section of WD ice with no chemical evidence of volcanic fallout, as well as two sets of filters representing the early and later stages during the extended volcanic period. All pairs of filters subsequently were back-flushed vigorously with ultra-pure water to release any captured particles; the back-flushed solution samples were filtered and then prepared for electron microprobe analysis following standard procedures for volcanic tephra analyses (21). Following targeted replicate coring efforts to recover two additional complete cores from this depth interval, tephra samples also were collected from the first three of nine total pulses of volcanic fallout in the overall ~192-year event. Small concentrations of silicate particles were detected for the depth interval corresponding to the early stages of the 17.7ka event (2430–2426 m). No glass shards were found in the background sample or in the sample corresponding to the later stages of the 17.7ka event, consistent with the continuous insoluble particle measurements (SI Appendix, Fig. S1). Most of the particles identified in the sample were fine (~10 μm), and some had cuspate shapes suggestive of volcanic origin. The geochemistry of individual glass shards was analyzed using a Cameca SX-100 electron microprobe [see methods in (21, 22)]. Results are summarized in Table S1.

Mt. Takahe, a heavily glaciated West Antarctic volcano, is characterized by an unusual, 8 km wide summit caldera (23). This feature is unique among West Antarctic stratovolcanoes and is unusual even in a global context. The flat-topped nature of Mt. Takahe initially was thought to be a result of completely sub-glacial volcanism, resulting in a characteristic “table mountain” form, but subsequent fieldwork revealed significant sub-aerial volcanism on the upper parts of the volcano, thereby ruling out sub-glacial origin (24). The flat-topped shape of Mt. Takahe remains enigmatic. Note that the halogen-rich and tephra-poor characteristics of the event fallout are similar to modern emissions from Mt. Erebus (25) and Mt. Etna. Because of the degree of glaciation, the chronological record of explosive volcanism at Mt. Takahe is incomplete. Explosive events have been dated at 8.2±5.4ka, 93.3±7.8ka, and 102±7.4ka (26). Eruptive events, sampled as lavas, also occurred at Mt. Takahe at 7±6, 29±12, 34±8, 39±14, 45±8, 50±15, and 104±28ka (27) so eruptive activity in the age range of 17.7ka is consistent with the volcano’s overall eruptive patterns.

Table S1. Major element composition of tephra shards from the main and replicate WD ice cores, with representative compositions for West Antarctic volcanoes Mt. Takahe and Mt. Berlin.

Depth Range m	n	P_2O_5	SiO_2	SO_2	TiO_2	Al_2O_3	MgO	CaO	MnO	FeO	Na_2O	K_2O
2430.0-2426.0 (WD main core)	4	0.29 (±0.02)	61.70 (±0.76)	0.25 (±0.05)	0.87 (±0.12)	14.98 (±0.31)	0.50 (±0.00)	2.10 (±0.09)	0.32 (±0.08)	8.89 (±0.18)	5.02 (±1.18)	4.66 (±0.22)
2426.05-2426.60 (Replicate core)	40	0.22 (±0.05)	60.54 (±0.74)	0.12 (±0.05)	0.87 (±0.08)	15.29 (±0.50)	0.54 (±0.11)	2.14 (±0.14)	0.32 (±0.06)	8.41 (±0.56)	6.31 (±0.61)	4.75 (±0.14)
2425.50-2426.30 (Replicate core)	27	0.25 (±0.05)	60.20 (±0.96)	0.13 (±0.06)	0.90 (±0.08)	15.24 (±0.58)	0.52 (±0.11)	2.11 (±0.35)	0.33 (±0.06)	8.78 (±0.61)	6.06 (±0.63)	4.79 (±0.37)
2425.75-2425.25 (Replicate core)	8	0.22 (±0.05)	61.11 (±0.69)	0.13 (±0.04)	0.83 (±0.12)	15.12 (±0.20)	0.55 (±0.12)	1.98 (±0.28)	0.32 (±0.04)	8.36 (±0.40)	6.17 (±0.52)	4.66 (±0.25)
Mt. Takahe		0.16	61.82	0.09	0.80	15.30	0.34	1.59	0.31	8.29	5.90	5.17
Mt. Berlin		0.04	62.57	0.08	0.52	13.88	0.00	1.03	0.26	8.84	7.69	4.69

Notes:

Geochemical quantities are in weight %. Analyses are normalized to 100 weight %. n equals number of analyses. Analytical precision based on replicate analyses of standard reference materials of similar composition to the unknowns (VG-568; KN-18; KE-12) are as follows (all in weight %): P_2O_5±0.02, SiO_2±0.47, SO_2±0.01, TiO_2±0.03, Al_2O_3±0.12, MgO±0.07, CaO±0.02, MnO±0.06, FeO±0.06, Na_2O±0.55, K_2O±0.27. Peak count times of 20 seconds were used for all elements with the exception of Na (40 seconds) and S (40 seconds). Primary calibration standards are: P_2O_5 and CaO Beeson apatite; SiO_2, K_2O, Al_2O_3 orth-1; TiO_2 rutile, MgO diopside, MnO MnO, FeO magnetite; Na_2O Amelia albite; SO_2 barite. Beam sizes used for analysis ranged between 10 and 15 μm, depending on the size of grain available. Replicate cores were sampled over depth ranges that contained individual volcanic pulses (Figs. 2, S1).

`

Mt. Takahe Emission Estimates

We estimated peak and average chlorine emissions during the ~192-year Mt. Takahe event based on the chlorine fallout measured in the WD, Byrd, and Taylor Glacier ice cores. Peak and average excess chlorine (observed fluxes minus background levels) at WD and Byrd (nearly identical at both sites) were ~74 and ~13 mg m^{-2} y^{-1}, respectively. At Taylor Glacier, peak and average fluxes were ~5.6 and ~1.5 mg m^{-2} y^{-1}, respectively. The WD, Byrd, and Taylor Glacier ice core sites are located approximately 350, 450, and 2000 km from Mt. Takahe, respectively. Assuming a radially symmetric, exponential drop off in fluxes away from the volcano results in peak chlorine emissions of ~400 Gg y^{-1}, with average emissions during the ~192-year event of 100 Gg y^{-1}. We emphasize that these only are order of magnitude estimates because so few measurements of the fallout are available. These levels are ~10 and ~40 times higher than modern emissions reported for nearby Mt. Erebus (28) and ~0.5 to ~2.5 times those reported for Mt. Etna (25). Mt. Etna currently is the largest point source in the world.

Reactive bromine is far more efficient than chlorine at destroying ozone in the stratosphere (29); but because bromine is reversibly deposited in the snowpack (SI Appendix – Snowpack Modeling), we were unable to use ice core measurements of fallout to estimate bromine emissions from the 17.7ka Mt. Takahe event. Assuming bromine-to-chlorine ratios as in modern emissions from Mt. Erebus (28), however, reactive bromine from Mt. Takahe likely also contributed to stratospheric ozone depletion.

`

Evidence for Reversible Bromine Deposition in Antarctic Snow

Evidence for reversible deposition of bromine and significant depletion can be found in modern Antarctic snowpacks. Sodium and bromine in Antarctic ice and snow derive primarily from ocean sources, but sodium is irreversibly deposited. Long-term average depositional fluxes for bromine and sodium measured in an array of 11 widely spaced ice cores from East and West Antarctica (7) are plotted against snowfall rate (SI Appendix, Fig. S4). This ice core array covers a broad range of snowfall rates ranging from 27 kg m^{-2} y^{-1} at NUS7-2 to 402 kg m^{-2} y^{-1} at DIV, and the chemical records span recent centuries to millennia. All of the core sites can be considered inland since all are located at least 200 km from the coast, so the snow chemistry is not heavily influenced by local marine sources.

SI Appendix, Fig. S4 shows depositional fluxes of bromine and sodium that were strongly dependent on snowfall rates. Using a simple linear model fit to the observed sodium flux versus snowfall (slope = 22.9 [±2.6]; intercept = -82 [±520]; R^2=0.945; $p < 0.0001$) shows that deposition was almost entirely through wet processes since the dry deposition term (intercept) is negligible when compared to the magnitude of the sodium concentrations. While bromine deposition also is well represented by this simple model (slope = 0.533 [±0.009]; intercept = -17.3 [±1.9]; R^2=0.999; $p < 0.0001$), the dry deposition term (intercept) is large relative to the wet deposition term (slope) and negative, indicating substantial release of bromine from the snowpack back to the atmosphere after deposition. That is, in modern snowpacks located both at high elevation, low-snowfall East Antarctic sites and lower elevation, high-snowfall West Antarctic sites, bromine was reversibly deposited with the initial flux to the surface linked to wet deposition processes. Concentrations preserved in the snow and ice were controlled almost entirely by the snowfall rate. Perhaps surprisingly, the re-emission rate does not appear to be related to the snow concentration as indicated by the very close fit (R^2=0.999) between the linear model and observations. For the mean snowfall rate in the array of 150 kg m^{-2} y^{-1}, >>99% of the sodium flux was through wet deposition based on the linear model, with no re-emission. For bromine, conversely, wet deposition was ~80 µg m^{-2} y^{-1}, but ~17 µg m^{-2} y^{-1} or about 22% was re-emitted into the atmosphere before the snow was buried, and the remaining bromine was preserved in the firn and ice. At sites with snowfall rates less than ~35 kg m^{-2} y^{-1}, nearly all bromine was re-emitted to the atmosphere prior to burial.

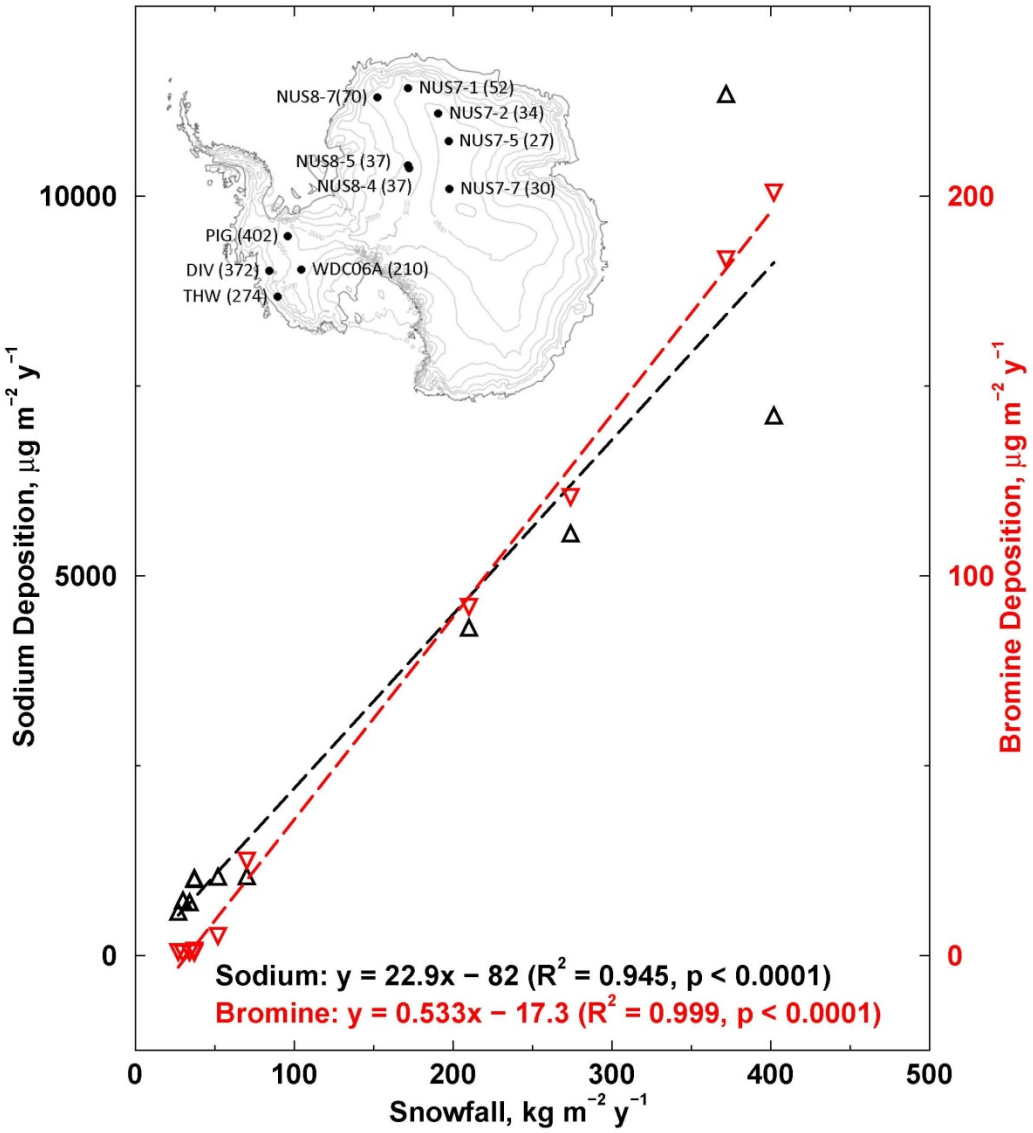

Fig. S4 Measurements of modern net deposition of bromine in an array of 11 Antarctic ice cores show the impact of reversible deposition. A linear model (dashed) fit to the average net deposition of sodium (black) and bromine (red) during recent centuries to millennia versus snowfall shows that while wet deposition accounts for nearly all of the flux of both elements (R^2 of 0.945 and 0.999 for sodium and bromine, respectively), bromine is reversibly deposited with a substantial portion (17.3±1.9 μg m^{-2} y^{-1}) re-emitted into the atmosphere prior to burial. Sodium is irreversibly deposited as shown by the small intercept compared to the measured concentrations. Inset shows the names and locations of the ice cores. Mean snowfall rates (kg m^{-2} y^{-1}) at each site are shown in parentheses.

`

Snowpack Modeling

The near-surface snowpack acts as a photochemical reactor (20, 30, 31), with a number of chemical species including reactive bromine and nitrate cycling between the air and snow. The result is substantial depletion in the snowpack if release into the atmosphere occurs more quickly than deposition followed by burial of the surface snow. The rate of release (loss) from the surface snow in part is determined by the duration and intensity of exposure of the snow to incoming UV radiation. Exposure duration is determined by the snow accumulation or burial rate since sunlight penetration below ~0.3 m (e-folding depth) in the snowpack is minimal (20). A large increase in UV radiation because of a decrease in the total ozone column will significantly increase exposure intensity during a fixed period of time, compared to the situation without a decrease in stratospheric ozone. Another possible factor determining bromine levels in surface snow may be acidity because the reactions that convert bromide into Br_2 that is subsequently released into the atmosphere are acid catalyzed (32).

The 17.7ka event in the WD and Byrd ice core record is characterized by sharp and sustained declines in bromine concentrations that occur with no detectable change in nitrate concentrations (Figs. 1) (SI Appendix, S1, S2). No anomalous increases in bromine concentration occurred at the start or end of the depletion, ruling out acidity-gradient-driven or other migration of bromine away from the 17.7ka anomaly, as has been reported for some ions (33). No change in snow accumulation was observed during the anomaly, indicating that there were no changes in exposure duration and pointing to increases in UV exposure intensity and possibly acidity increases as the likely cause of bromine loss during these events.

To evaluate the contribution of two factors on bromine and nitrate loss – (1) an increase in incoming UV radiation due to a reduction in stratospheric ozone, and (2) an increase in surface snowpack acidity – we used the 1-D coupled model of snow-atmosphere photochemistry MISTRA-SNOW. SI Appendix, Fig. S5 shows changes in bromine and nitrate concentrations in surface snow above an idealized 2 m snow column during a 72-hour model simulation. Initial concentrations at the surface are similar to those found today in the snow at WD, and concentrations decline exponentially from the surface.

For the control simulation, we used a typical modern total atmospheric ozone column burden of 300 Dobson Units (DU) with bulk acidity concentrations similar to those measured in the WD ice core. After 72 hours, average bromine concentrations in the surface-snow layer (0.01 m) and upper 1.0 m declined by ~7.8% and ~5.7%, respectively (SI Appendix, Fig. S5). Similarly, nitrate concentrations declined by ~3.3% in the surface snow and ~2.4% in the upper 1.0 m.

To evaluate sensitivity to atmospheric ozone changes, we repeated the control simulation but with total column ozone burdens varying from 50 to 250 DU (SI Appendix, Fig. S5). Re-emission of bromine increased with decreasing ozone burden, with approximately two-fold and three-fold increases in bromine loss for 50 DU compared with 300 DU for the surface-snow layer and upper 1.0 m of the snowpack, respectively. Nitrate losses also were sensitive to decreasing ozone burden but not nearly as sensitive as bromine.

`

Bromine and nitrate loss from the near-surface snowpack also may be sensitive to acidity concentrations through pH-dependent changes in reaction rates. To evaluate the sensitivity to acidity, we repeated the simulations but with two times the initial bulk H^+ concentrations and found substantially greater loss of bromine from both the surface snow and snowpack for all levels of total column ozone. Acid concentrations had little impact on nitrate loss in the model simulations. Taken together, the snowpack photochemistry model simulations suggest that bromine loss from the snow is more rapid than nitrate and that it is more sensitive to changes in total ozone column burden than acidity. In addition, simulations indicate that increasing the acidity of the snowpack enhances bromine loss for all ozone burdens but has little impact on nitrate loss. Thus, the lack of significant change in nitrate concentration observed during the 17.7ka event is consistent with ozone-hole-related changes in UV radiation.

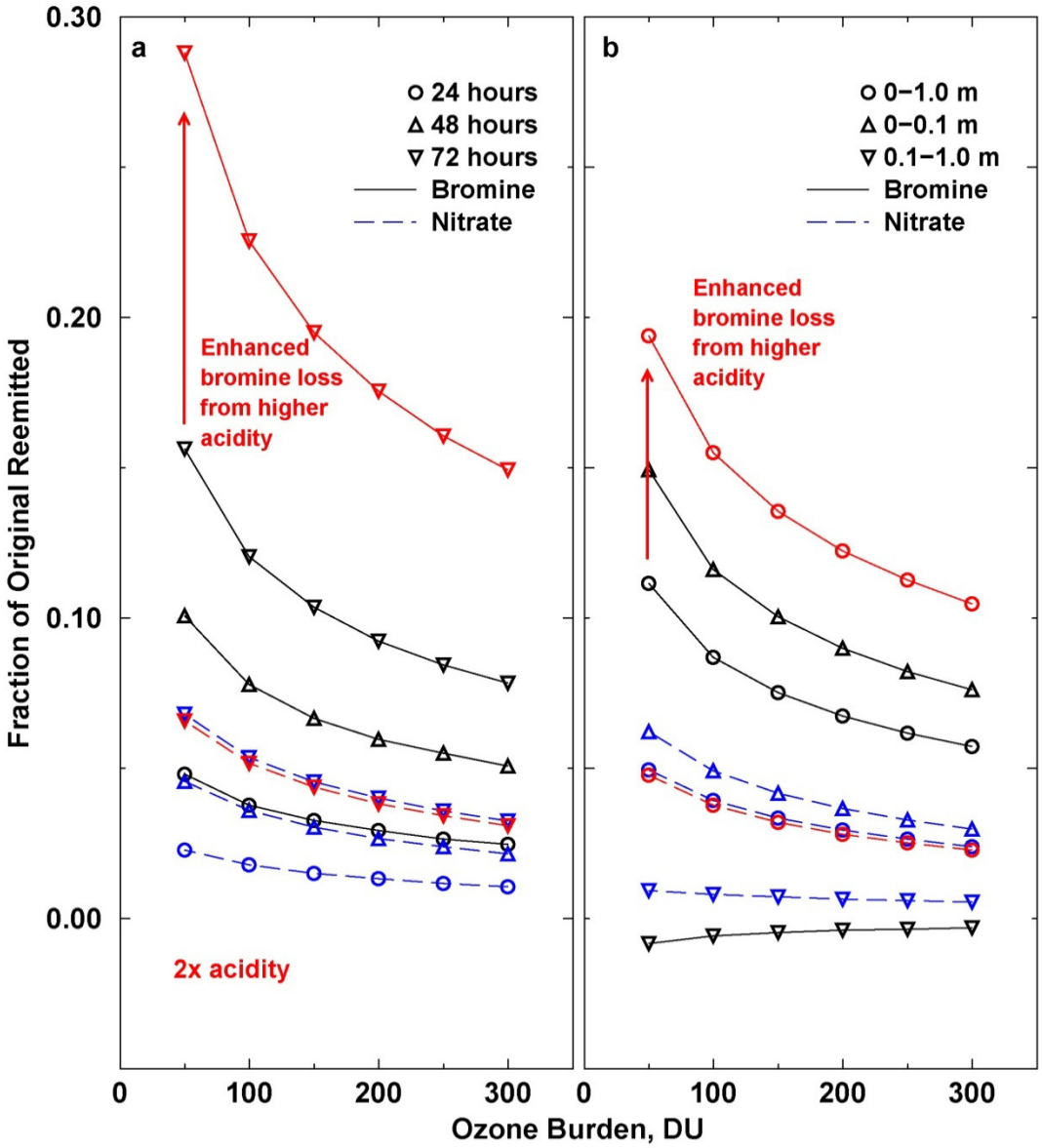

Fig. S5 MISTRA-SNOW (18) snowpack photochemistry model simulations of reversible deposition for bromine and nitrate in an idealized snowpack for different levels of total column ozone burden. (**a):** Simulations of bromine and nitrate emissions to the atmosphere from the surface-snow layer. (**b):** Simulations for the upper 1 m of the snowpack. Although nitrate re-emission from the surface snow and snowpack increases with decreased ozone burden, increases are much larger for bromine. Moreover, increased acidity (shown in red) has little or no impact on the re-emission rate of nitrate but substantial impact on bromine since associated reactions are acid catalyzed.

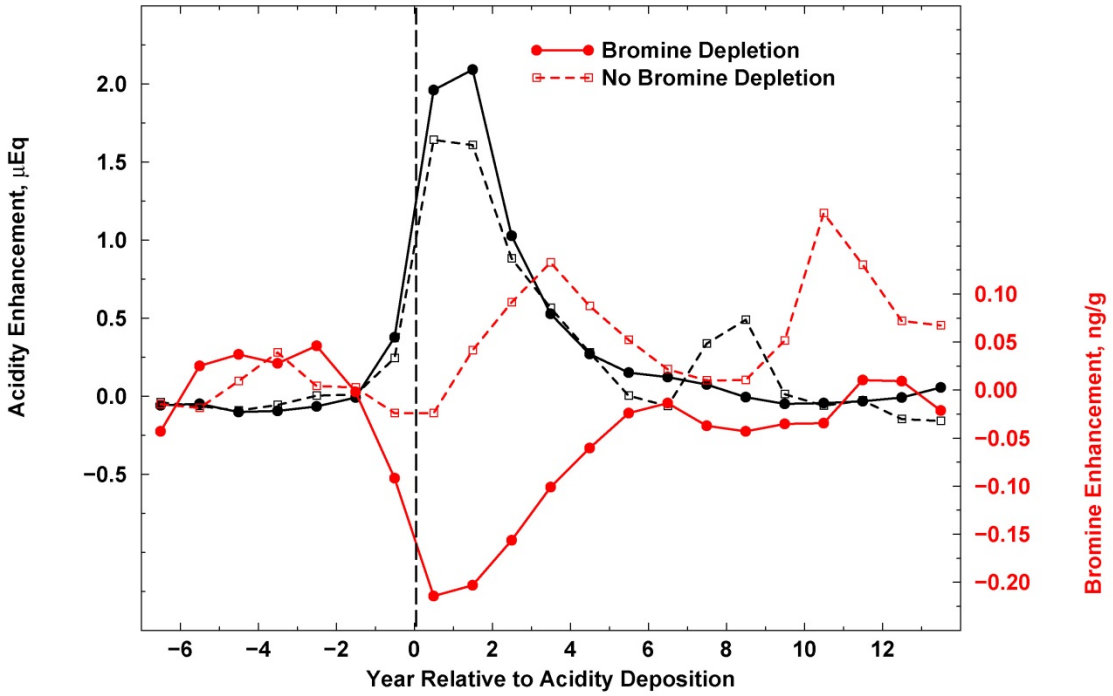

Fig. S6 Superposed epoch analysis for the 100 high acidity events between 10ka and 25ka in the WD ice core. All fallout events with annual average acidity concentrations >3.0 µeq L^{-1} (µEq) were included except those during the 17.7ka Mt. Takahe event. Shown are stacked acidity and bromine concentration enhancements, with enhancement defined as the annual concentration minus the average during the seven years preceding the start of enhanced acid deposition. Of the 100 events, 30 showed no bromine depletion on average during the four years following the start of enhanced acid deposition and corresponding to the period of highest acidity. Even though acid concentrations were similar for events with and without bromine depletion, the lack of bromine depletion for 30% of the events clearly demonstrates that high snow acidity alone is not sufficient to cause bromine depletion. Results also suggest that about 70% of large volcanic eruptions during this period were associated with stratospheric ozone loss that led to enhanced surface UV and loss of bromine from the snow, consistent with studies showing that many, but not all, modern eruptions result in measureable stratospheric ozone depletion (1, 2).

`

Comparisons to Modern Ozone Depletion

The seasonality and duration of increased surface UV from modern ozone depletion and the postulated 17.7ka ozone depletion may have been different. Modern chlorofluorocarbon-driven ozone loss and increased surface UV largely are springtime phenomena since increased UV persists only from sunrise until the Antarctic stratosphere isolated by the strong winter polar vortex mixes with mid- and low-latitude air as the vortex breaks down. For the postulated 17.7ka ozone hole, however, the source volcano was at 76^{o}S and presumably erupting throughout the year. While stratospheric halogen and sulfur concentrations may have been somewhat reduced by a weakened summertime vortex, the paleo-ozone hole likely persisted throughout the austral summer, leading to much greater integrated UV exposure each year and thus greater bromine loss.

Demonstrating enhanced bromine loss in near-surface snow in response to the modern anthropogenic ozone depletion requires a suitable ice core record. First, it is clear from modern observations (e.g., SI Appendix, Fig. S4) and snowpack photochemical modeling that bromine is reversibly deposited in polar snow. Most of the originally deposited bromine will be re-emitted to the atmosphere at low accumulation sites even under normal UV illumination, while bromine concentrations preserved in snow at high accumulation sites will be relatively insensitive to enhanced UV because the snow will be buried and cut off from UV and ventilation too quickly for significant UV-enhanced re-emission to occur. The ideal accumulation rate seems to be 100 kg/m^2/y based on the WD record. Second, because of the strong dependence of preserved bromine concentration on snow accumulation, any ice core record useful for assessing the impact of modern ozone depletion must show constant snow accumulation for at least the past 200 years to avoid accumulation-driven concentration changes and provide a robust record of background bromine prior to and during stratospheric ozone loss. Third, snowpack modeling (SI Appendix, Fig. S5) shows that UV-driven bromine re-emission is enhanced at higher acidities, and no evidence for increased acidity in Antarctica has been found during this period. Fourth, sea ice variability may alter bromine emissions and deposition to snow nearby, so suitable cores must be located well away from shorelines. To our knowledge, no Antarctic ice core records of bromine that match these criteria exist.

`

Atmosphere Ocean General Circulation Model Simulations

Observations and modeling indicate that the modern anthropogenic ozone hole has altered hydroclimate throughout the SH – including changes in atmospheric (34) and therefore oceanic circulation (34, 35), surface temperature (34), and precipitation (36-38). Specifically for precipitation, prescribed ozone depletion in model simulations resulted in a southward shift in Hadley circulation and the extra-tropical westerly jet (36), leading to subtropical moistening and mid-latitude drying similar to recent observations (Fig. 5). Increasing greenhouse gas concentrations are thought to have a broadly similar impact on SH climate, confounding the attribution of recent climate changes (39).

To evaluate the potential climate impact of a springtime ozone hole ~17.7k years ago, we used the COSMOS coupled Atmosphere Ocean General Circulation Model (AOGCM) initialized to Last Glacial Maximum (LGM) environmental conditions (40). The atmosphere model component ECHAM5 (41) was used at T31 resolution (~3.75°) with 19 vertical levels. The ocean component was MPIOM (42) with a curvilinear Arakawa-C grid and a formal horizontal resolution of ~1.8º x 3º. Forty unevenly spaced layers represented the vertical domain. For the ozone hole simulation, ozone concentrations from September through December each year were modified from standard levels (>1 ppmv) to 0.1 ppmv in height layers above 50 hPa over the latitude range 60^{o}S to 90^{o}S, since similar patterns of springtime ozone depletion have been observed during the modern ozone hole (43). This simulation with ozone depletion extended for 200 years.

Comparisons between 100-year averages of net precipitation (precipitation minus evaporation or P-E), 10 m wind velocity, and surface air temperature with the initial LGM climate and during the last 100 years of the 200-year ozone-hole simulation indicate that springtime ozone depletion could have had significant impacts on SH climate. Simulated changes in zonally averaged net precipitation (SI Appendix, Fig. S7) are similar both in latitudinal pattern and magnitude to those ascribed to modern stratospheric ozone depletion. Specifically, the model simulates drier conditions from ~6^{o} to ~22^{o}S and from ~41^{o} to ~58^{o}S, with moistening from ~22^{o} to ~41^{o}S and south of ~58^{o}S. As with the modern ozone hole (44), westerly winds in the region of the Drake Passage increase, with zonally averaged winds at 60^{o}S increasing 5% to 10% particularly during austral summer (DFJ) (SI Appendix, Fig. S7). The magnitude of the wind increase at 60^{o}S, however, is lower in the LGM simulation.

Temperatures also change in the 60^{o}S region particularly in the Pacific and Atlantic sectors, with simulated long-term (>100 year), quasi-equilibrium increases in annual LGM surface temperatures of 0.4^{o} to 0.8^{o} C as a result of ozone depletion (SI Appendix, Fig. S7). These increases are in agreement with modern quasi-equilibrium warming simulated using a coarse (1^{o}) model resolution (45), although similar experiments using a finer (0.1^{o}) model resolution simulated cooling over Antarctica but warming over the Southern Ocean (45). Additional published model simulations suggest a two-stage response to modern ozone depletion (46) – initial transient cooling followed by slower (decadal-scale) warming. The quasi-equilibrium

`

LGM responses reported here should not be confused with transient responses simulated for modern stratospheric ozone depletion (47).

The AOGCM-simulated changes in climate driven by persistent ozone depletion during the LGM also provide a possible means to change ventilation of the deep ocean around Antarctica exactly at the time hypothesized by Schmitt et al. (48) (Figs. 1, 2) to explain large changes in atmospheric CO_2 and stable carbon isotopes of CO_2 and increased upwelling. These include increases in the westerly wind belt around Antarctica and warming, particularly in the Pacific and Atlantic sectors of coastal Antarctica.

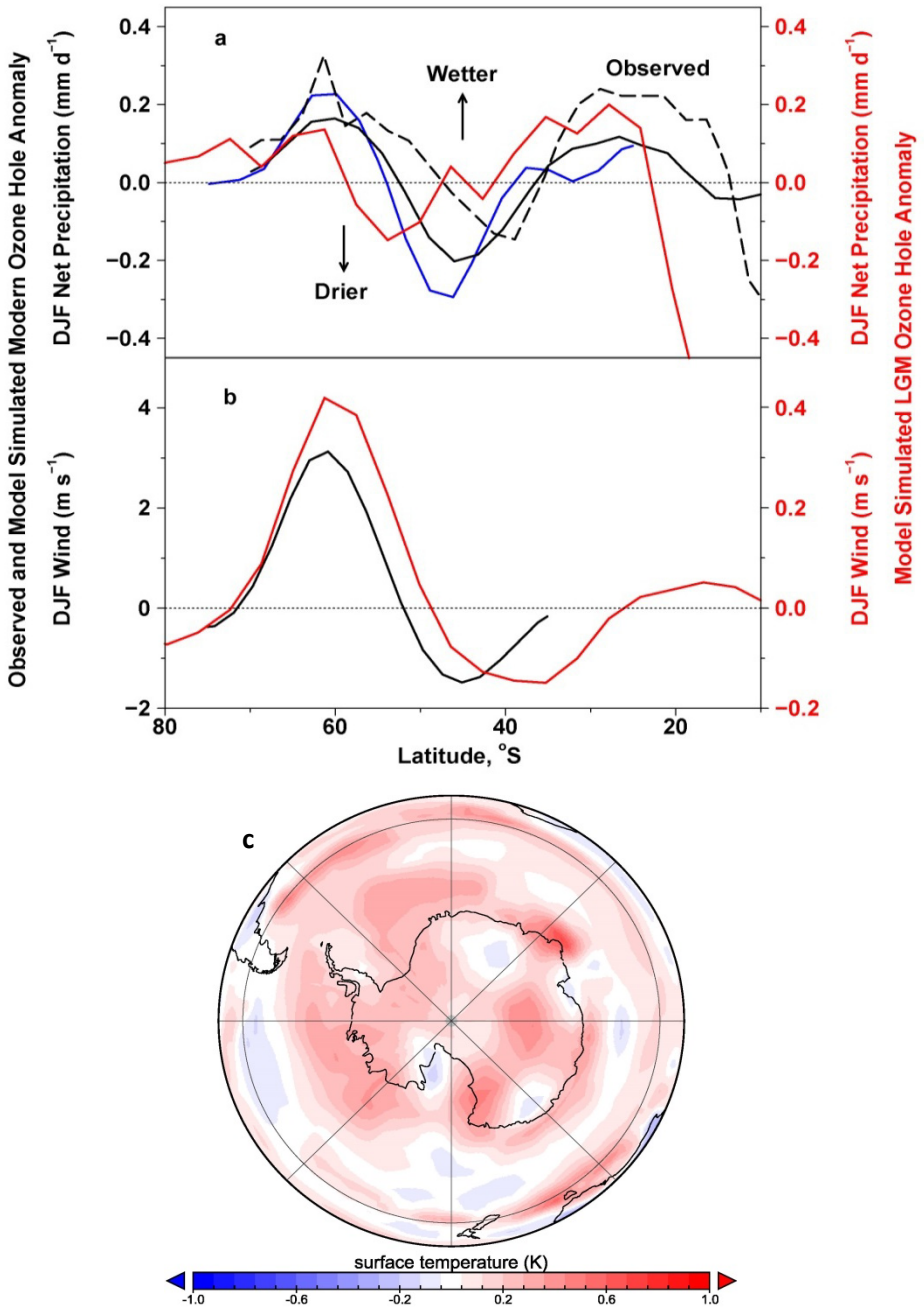

Fig. S7 Observed and model-simulated austral summer anomalies in hydroclimate associated with modern and postulated 17.7ka stratospheric ozone depletion. (a): Observed (black dashed (36) and modeled (modern: blue (38) and black (36) solid, LGM: red) zonal average changes in austral summer precipitation**. (b):** Modeled (modern: black (38); LGM: red) zonal average changes in wind. **(c):** Simulated austral summer average surface temperature anomalies resulting from the 17.7ka ozone hole. Simulated hydroclimatic responses to stratospheric ozone depletion under LGM conditions qualitatively are similar to observations and modeling of the modern ozone hole, but changes in winds are muted.

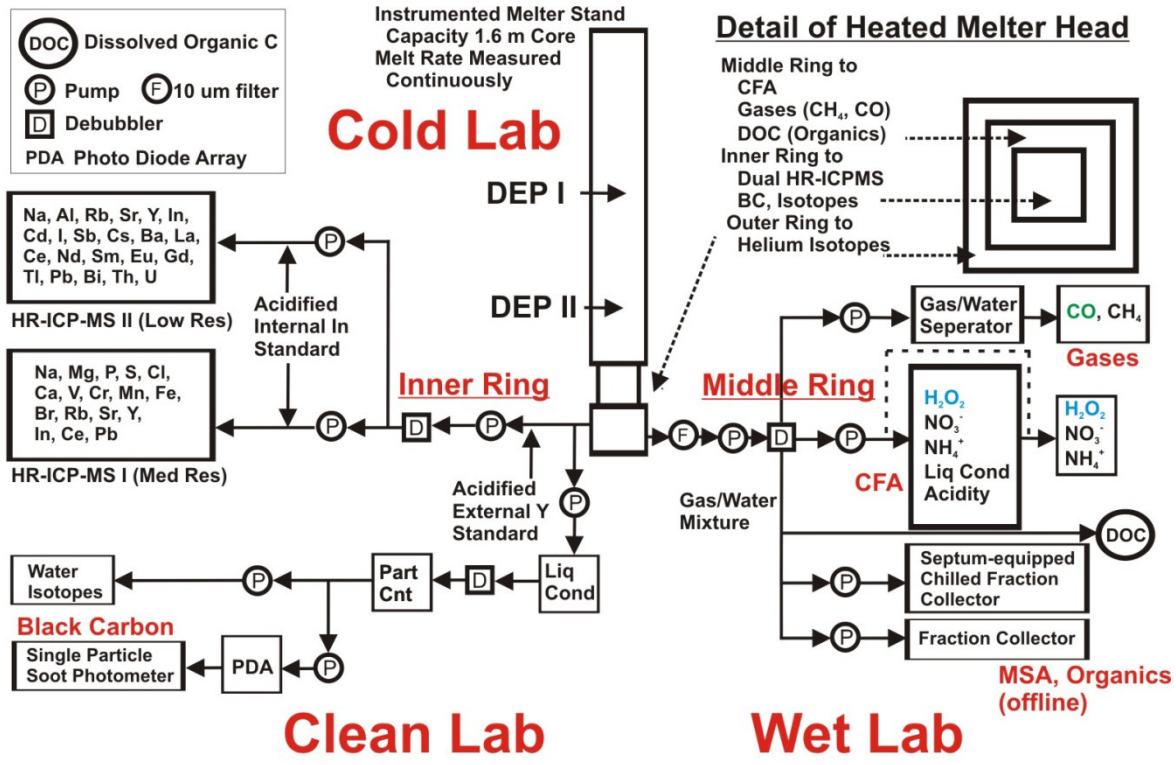

Fig. S8 Schematic of the CFA-TE-BC-GAS analytical system used for high-resolution, continuous analyses of WD, Byrd, and other ice cores. For replicate analysis of the 17.7ka event in the WD core, 10 µm filters were added to the lines coming from the middle ring to capture tephra for single-particle microprobe analyses. Discrete samples were collected during the continuous analyses for subsequent measurements of helium isotopes and chemical species such as fluoride and bromide. Hydrogen peroxide (H_2O_2) was not measured below 2171 m.

`

SI Appendix References

1. Kutterolf S*, et al.* (2013) Combined bromine and chlorine release from large explosive volcanic eruptions: A threat to stratospheric ozone? *Geology* 41(6):707-710.
2. Solomon S*, et al.* (2016) Emergence of healing in the Antarctic ozone layer. *Science* 353(6296):269-274.
3. Banta JR, McConnell JR, Frey MM, Bales RC, & Taylor K (2008) Spatial and temporal variability in snow accumulation at the West Antarctic Ice Sheet Divide over recent centuries. *J. Geophys. Res.-Atmos.* 113(D23).
4. Hammer CU, Clausen HB, & Langway CC (1997) 50,000 years of recorded global volcanism. *Climatic Change* 35(1):1-15.
5. Baggenstos D (2015) Taylor Glacier as an archive of ancient ice for large-volume samples: Chronology, gases, dust, and climate. Ph.D. (University of California, San Diego).
6. McConnell JR (2002) Continuous ice-core chemical analyses using inductively Coupled Plasma Mass Spectrometry. *Environmental Science & Technology* 36(1):7-11.
7. McConnell JR*, et al.* (2014) Antarctic-wide array of high-resolution ice core records reveals pervasive lead pollution began in 1889 and persists today. *Scientific Reports* 4(5848):1-5.
8. McConnell JR & Edwards R (2008) Coal burning leaves toxic heavy metal legacy in the Arctic. *Proceedings of the National Academy of Sciences of the United States of America* 105(34):12140-12144.
9. Sigl M*, et al.* (2016) The WAIS Divide deep ice core WD2014 chronology - Part 2: Annual-layer counting (0-31 ka BP). *Clim. Past* 12:769-786.
10. McConnell JR*, et al.* (2007) 20th-century industrial black carbon emissions altered arctic climate forcing. *Science* 317(5843):1381-1384.
11. McConnell JR, Aristarain AJ, Banta JR, Edwards PR, & Simoes JC (2007) 20th-century doubling in dust archived in an Antarctic Peninsula ice core parallels climate change and desertification in South America. *Proceedings of the National Academy of Sciences of the United States of America* 104(14):5743-5748.
12. Sigl M*, et al.* (2015) Timing and climate forcing of volcanic eruptions for the past 2,500 years. *Nature* 523(7562):543-549.
13. Pasteris DR, McConnell JR, & Edwards R (2012) High-resolution, continuous method for measurement of acidity in ice cores. *Environmental Science & Technology* 46(3):1659-1666.
14. Rhodes RH*, et al.* (2015) Enhanced tropical methane production in response to iceberg discharge in the North Atlantic. *Science* 348(6238):1016-1019.
15. Rhodes R, Baker J, Millet M, & Bertler N (2011) Experimental investigation of the effects of mineral dust on the reproducibility and accuracy of ice core trace element analyses. *Chemical Geology* 286(3-4):207-221.
16. Maselli OJ*, et al.* (2017) Sea ice and pollution-modulated changes in Greenland ice core methanesulfonate and bromine. *Climate of the Past* 13:39-59.
17. Paris G, Sessions AL, Subhas AV, & Adkins JF (2013) MC-ICP-MS measurement of delta S-34 and Delta S-33 in small amounts of dissolved sulfate. *Chemical Geology* 345:50-61.

`

18. Thomas JL*, et al.* (2011) Modeling chemistry in and above snow at Summit, Greenland - Part 1: Model description and results. *Atmospheric Chemistry and Physics* 11(10):4899-4914.
19. Dibb JE, Ziemba LD, Luxford J, & Beckman P (2010) Bromide and other ions in the snow, firn air, and atmospheric boundary layer at Summit during GSHOX. *Atmospheric Chemistry and Physics* 10(20):9931-9942.
20. France JL*, et al.* (2011) Snow optical properties at Dome C (Concordia), Antarctica; implications for snow emissions and snow chemistry of reactive nitrogen. *Atmospheric Chemistry and Physics* 11(18):9787-9801.
21. Dunbar NW, Zielinski GA, & Voisins DT (2003) Tephra layers in the Siple Dome and Taylor Dome ice cores, Antarctica: Sources and correlations. *Journal of Geophysical Research-Solid Earth* 108(B8):11.
22. Dunbar NW, McIntosh WC, & Esser RP (2008) Physical setting and tephrochronology of the summit caldera ice record at Mount Moulton, West Antarctica. *Geological Society of America Bulletin* 120(7-8).
23. Palais JM, Kyle PR, McIntosh WC, & Seward D (1988) Magmatic and phreatomagmatic volcanic activity at Mt Takahe, West Antarctica,based on tephra layers in the Byrd ice core and field observations at Mt Takahe. *Journal of Volcanology and Geothermal Research* 35(4).
24. McIntosh WC, LeMasurier WE, Ellerman PJ, & Dunbar NW (1985) A reinterpretation of glaciovolcanic interaction at Mount Takahe and Mount Murphy, Marie Byrd Land, Antarctica. *Antarctic Journal of the United States* 19:57-59.
25. Francis P, Burton MR, & Oppenheimer C (1998) Remote measurements of volcanic gas compositions by solar occultation spectroscopy. *Nature* 396(6711):567-570.
26. Wilch TI, McIntosh WC, & Dunbar NW (1999) Late Quaternary volcanic activity in Marie Byrd Land: Potential Ar-40/Ar-39-dated time horizons in West Antarctic ice and marine cores. *Geological Society of America Bulletin* 111(10).
27. Wilch TJ (1997) Volcanic record of the West Antarctic ice sheet in Marie Byrd Land. (New Mexico Institute of Mining and Technology, Socorro).
28. Zredagostynska G, Kyle PR, & Finnegan DL (1993) Chlorine, fluorine, and sulfur emissions from Mount Erebus, Antarctica and estimated contribution to the Antarctic atmosphere. *Geophysical Research Letters* 20(18):1959-1962.
29. Cadoux A, Scaillet B, Bekki S, Oppenheimer C, & Druitt T (2015) Stratospheric ozone destruction by the Bronze-Age Minoan eruption (Santorini Volcano, Greece). *Scientific Reports* 5.
30. Anderson RF*, et al.* (2009) Wind-driven upwelling in the Southern Ocean and the deglacial rise in atmospheric CO^2. *Science* 323(5920).
31. Abbatt JPD*, et al.* (2012) Halogen activation via interactions with environmental ice and snow in the polar lower troposphere and other regions. *Atmos. Chem. Phys.* 12(14):6237-6271.
32. Mozurkewich M (1995) Mechanisms for the release of halogens from sea-salt particles by free-radical reactions. *Journal of Geophysical Research-Atmospheres* 100(D7):14199-14207.
33. Traversi R*, et al.* (2009) Study of Dome C site (East Antartica) variability by comparing chemical stratigraphies. *Microchemical Journal* 92(1):7-14.

`

34. Thompson DWJ*, et al.* (2011) Signatures of the Antarctic ozone hole in Southern Hemisphere surface climate change. *Nature Geoscience* 4(11):741-749.
35. Waugh DW, Primeau F, DeVries T, & Holzer M (2013) Recent changes in the ventilation of the southern oceans. *Science* 339(6119):568-570.
36. Kang SM, Polvani LM, Fyfe JC, & Sigmond M (2011) Impact of polar ozone depletion on subtropical precipitation. *Science* 332(6032):951-954.
37. Gonzalez PM, Polvani L, Seager R, & Correa GP (2013) Stratospheric ozone depletion: a key driver of recent precipitation trends in South Eastern South America. *Climate Dynamics*:1-18.
38. Polvani LM, Waugh DW, Correa GJP, & Son S-W (2011) Stratospheric ozone depletion: The main driver of twentieth-century atmospheric circulation changes in the Southern Hemisphere. *Journal of Climate* 24(3):795-812.
39. Son SW*, et al.* (2008) The impact of stratospheric ozone recovery on the Southern Hemisphere westerly jet. *Science* 320(5882):1486-1489.
40. Zhang X, Lohmann G, Knorr G, & Xu X (2013) Different ocean states and transient characteristics in Last Glacial Maximum simulations and implications for deglaciation. *Climate of the Past* 9(5):2319-2333.
41. Roeckner E*, et al.* (2006) Sensitivity of simulated climate to horizontal and vertical resolution in the ECHAM5 atmosphere model. *Journal of Climate* 19(16):3771-3791.
42. Marsland SJ, Haak H, Jungclaus JH, Latif M, & Roske F (2003) The Max-Planck-Institute global ocean/sea ice model with orthogonal curvilinear coordinates. *Ocean Modelling* 5(2):91-127.
43. WMO (2011) Global Ozone Research and Monitoring Project—Report No. 52. in *Scientific Assessment of Ozone Depletion: 2010*.
44. Thompson DWJ & Solomon S (2002) Interpretation of recent Southern Hemisphere climate change. *Science* 296(5569).
45. Bitz CM & Polvani LM (2012) Antarctic climate response to stratospheric ozone depletion in a fine resolution ocean climate model. *Geophysical Research Letters* 39.
46. Ferreira D, Marshall J, Bitz C, Solomon S, & Plumb A (2015) Antarctic Ocean and sea ice response to ozone depletion: A two-time-scale problem. *Journal of Climate* 28(3):1206-1226.
47. Solomon A, Polvani L, Smith K, & Abernathey R (2015) The impact of ozone depleting substances on the circulation, temperature, and salinity of the Southern Ocean: An attribution study with CESM1(WACCM). *Geophysical Research Letters* 42(13):5547-5555.
48. Schmitt J*, et al.* (2012) Carbon isotope constraints on the deglacial CO^2 rise from ice cores. *Science* 336(6082).